A trap mutant reveals the physiological client spectrum of TRC40

Javier Coy-Vergara[1§], Jhon Rivera-Monroy[1§], Henning Urlaub[2,3], Christof Lenz[2,3] and Blanche Schwappach[1, 4,*]

[1]Department of Molecular Biology, University Medical Center Göttingen, Göttingen, Germany
[2]Bioanalytical Mass Spectrometry Group, Max Planck Institute for Biophysical Chemistry, Göttingen, Germany
[3]Bioanalytics Group, Institute of Clinical Chemistry, University Medical Center Göttingen, Göttingen, Germany
[4]Max Planck Institute for Biophysical Chemistry, Göttingen, Germany

§ These authors contributed equally to the work
* Corresponding author

Blanche Schwappach
Tel.: +49 551 395961
Fax: +49 551 395960
E-mail: blanche.schwappach@med.uni-goettingen.de

Summary statement: A strategy to decipher which tail-anchored proteins do (as opposed to can or must) use the TRC pathway in intact cells generates a comprehensive list of human TRC40 clients.

JCS Advance Online Article. Posted on 10 June 2019

Abstract

The TRC pathway targets tail-anchored (TA) proteins to the membrane of the endoplasmic reticulum (ER). While many TA-proteins are known to be able to use this pathway, it is essential for the targeting of only a few. Here, we uncover a large number of TA-proteins that engage with TRC40 when other targeting machineries are fully operational. We use a dominant negative, ATPase-impaired, mutant of TRC40 in which aspartate 74 was substituted by glutamate to trap TA-proteins in the cytoplasm. Manipulation of TRC40's hydrophobic TA-binding groove reduces interaction with most but not all substrates suggesting that co-purification may also reflect interactions unrelated to precursor protein targeting. We confirm known TRC40 substrates and identify many additional TA-proteins interacting with TRC40. Using the trap approach in combination with quantitative mass spectrometry, we show that Golgi-resident TA-proteins such as the golgins golgin-84, CASP, and giantin as well as the vesicle-associated membrane-protein-associated proteins VAPA and VAPB interact with TRC40. Thus, our results provide new avenues to tackle the essential role of TRC40 in metazoan organisms.

Introduction

The presence of membrane proteins customizes biological membranes to suit their respective functions beyond the formation of a permeability barrier. Membrane proteins enable transmembrane transport, modify the lipid environment, or mediate membrane contacts. This is true for the plasma membrane as well as for the many intracellular membranes enclosing subcellular compartments. The integration of a protein into a membrane-forming lipid bilayer is a feat of nature since protein biogenesis occurs in the aqueous phase. Investigation of the cellular machineries that enable the integration of proteins into membranes is as much a classical area as a current focus of molecular cell biology.

Reductionist approaches afford tremendous insights into the fundamentals of membrane integration of proteins. In fact, *in-vitro* reconstitution (Kutay et al., 1995; Stefanovic and Hegde, 2007) and the theoretical, physicochemical analysis of transmembrane segments (TMS) (von Heijne, 2007) have enabled the field to formulate detailed hypotheses about rules that govern membrane integration of proteins. In parallel, systematic strategies have uncovered several different protein complexes and pathways involved in membrane targeting at large (Aviram et al., 2016; Nguyen et al., 2018; Schuldiner et al., 2008; Shurtleff et al., 2018). These discoveries raise questions with regard to redundancy (which may be in place to achieve robustness), tissue specificity (which may optimize the physiological function of specialized cell types), and hierarchy of different membrane protein targeting pathways. Investigation of different cell types by physiologically-minded *in-vivo* approaches has revealed that some substrates are particularly sensitive to the loss of a specific pathway (Casson et al., 2017; Norlin et al., 2016; Rivera-Monroy et al., 2016).

An interesting example is provided by the topologically defined class of tail-anchored (TA) proteins that comprise one hydrophobic TMS at the C-terminus that anchors the protein in the membrane. The cytoplasmic N-terminus endows such proteins with their diverse functions, e.g. in vesicular traffic (most SNARE proteins are TA-proteins) whereas the luminal C-terminus does not exceed 40 amino acids (Borgese et al., 2003; Kutay et al., 1993). TA-proteins occur on all membranes facing the cytoplasm. The TA-proteins found in the contiguous secretory pathway, plasma membrane, and endo-lysosomal system are thought to be integrated into the membrane of the endoplasmic reticulum (ER) before they reach their respective locales by vesicular traffic (Borgese et al., 2007; Jäntti et al., 1994; Kutay et al., 1995; Linstedt et al., 1995; Pedrazzini et al., 1996).

The yeast GET or mammalian TRC pathway has been identified as a highly conserved cellular pathway capable of targeting the class of TA-proteins to the ER (Favaloro et al., 2008; Mariappan et al., 2010; Schuldiner et al., 2008; Stefanovic and Hegde, 2007). A plethora of complementary data from systematic genetic analyses in yeast (Jonikas et al., 2009; Schuldiner et al., 2008), *in-vitro* biochemical dissection (Bozkurt et al., 2009; Favaloro et al., 2008; Favaloro et al., 2010; Stefanovic and Hegde, 2007), and numerous crystal structures (Bozkurt et al., 2009; Gristick et al., 2014; Hu et al., 2009; Kubota et al., 2012; Mateja et al., 2009; Mateja et al., 2015; Simpson et al., 2010; Stefer et al., 2011; Yamagata et al., 2010) have helped generate the current model of TRC pathway function. Yet, it has become equally clear that *in vivo* the TA-proteins destined for the ER have several additional targeting options, such as the signal recognition particle (SRP) system (Abell et al., 2004; Abell et al., 2007; Casson et al., 2017), the SRP-independent targeting (SND) components (Aviram et al., 2016; Haßdenteufel et al., 2017), or the ER membrane complex (EMC) (Guna et al., 2018; Shurtleff et al., 2018). Hence, it is necessary to carefully distinguish which TA-proteins *can* use the TRC pathway from the precursors for which it is *essential*. While the existing tools such as *in-vitro* assays and knockout cells or organisms have begun to provide answers to these questions (Casson et al., 2017; Figueiredo Costa et al., 2018; Guna et al., 2018; Haßdenteufel et al., 2017; Lin et al., 2016; Norlin et al., 2016; Norlin et al., 2018; Pfaff et al., 2016; Rivera-Monroy et al., 2016; Vogl et al., 2016), an approach is still lacking that would reveal which TA-proteins *do* in fact use the TRC pathway when all targeting options are operational, i.e. without the compensatory effects often provoked by knockout strategies.

Here, we present a novel strategy to tackle this problem. Based on the ATPase cycle of TRC40, we designed and characterized a dominant negative "trap" mutant of TRC40, which accumulates TRC40-interacting precursor TA-proteins in the cytoplasm. This approach helped us to confirm known substrates of the pathway, to distinguish precursors that *can but do not have to* use TRC40-dependent membrane integration, and to test a large spectrum of endogenously expressed TA-proteins for their capacity to interact with TRC40 in the intact cellular environment. In addition, unbiased analysis of the TRC40 trap mutant's interactome by label-free quantitative mass spectrometry identified more than ten TA-proteins interacting with TRC40. Among these newly identified and subsequently verified TA-proteins are golgins such as golgin-84, CASP, and giantin. Golgins are central to the organization and functionality of the Golgi apparatus (Gillingham and Munro, 2016). Given the crucial role of giantin in the posttranslational modification of secretory proteins by glycosylation (Lan et al., 2016; McGee et al., 2017; Stevenson et al., 2017) our finding may help explaining the poorly understood

essentiality of the TRC pathway in mammals. At the same time, our data suggest that the observed co-purification of TA-proteins with TRC40 may partially reflect a molecular interaction unrelated to precursor protein targeting. Hence, our analysis motivates future focus on the chaperone function of proteins homologous to TRC40 and its yeast counterpart Get3 (Farkas et al., 2019).

Results

Steady-state levels of TA-proteins upon combined WRB and TRC40 depletion report on TRC pathway substrates with limited fidelity

Cellular quality control promotes the degradation of membrane protein precursors that mislocalize because their preferred targeting pathway is not operational (reviewed in Guna and Hegde, 2018). This consequence of mistargeting has been exploited to interpret the reduced steady-state levels of a TA-protein upon knockout or siRNA-mediated knockdown of TRC pathway components as evidence for the targeting of the respective substrate via TRC40 (Casson et al., 2017; Haßdenteufel et al., 2017; Norlin et al., 2016; Rivera-Monroy et al., 2016). In combination with *in-vitro* insertion assays, which answer the question whether a given substrate *can* target to the membrane of the ER via a TRC40 and WRB/CAML-dependent route, the results of this approach have been useful to identify substrates of the pathway, for which it is *obligatory*, such as syntaxins Stx5 and Stx6 as well as emerin (EMD) (Norlin et al., 2016; Pfaff et al., 2016; Rivera-Monroy et al., 2016).

Using this strategy in HeLa cells, we assessed the steady-state levels of TA-proteins that were implied by *in-vitro* assays as TRC pathway dependent substrates but not definitively and systematically tested as substrates in intact cells (Fig. 1). Substantial knockdown of *TRC40* and *WRB* was achieved (Fig. 1A,B) and the combined transfection with siRNAs directed against TRC40 and WRB resulted in a robust reduction of the TRC40 ATPase and both TRC40-receptor proteins, WRB and CAML. In effect, this manipulation leads to a knockout of the membrane targeting phase of the TRC40 cycle, in line with results obtained from the analysis of a *Wrb*-knockout mouse (Rivera-Monroy et al., 2016). As a positive control, we recapitulated TA-protein substrates known to depend on the TRC pathway *in vivo* such as Stx5, Stx6 and EMD, which showed reduced steady-state levels but also aberrant subcellular localization when the pathway is impaired (Norlin et al., 2016; Pfaff et al., 2016; Rivera-Monroy et al., 2016).

Indeed, the steady-state levels of all three substrates in the membrane fraction were strongly reduced (Fig. 1C,D) upon down-regulation of *TRC40* and *WRB*.

Next, we tested two TA-proteins, Sec61β, Sec22b, and Stx8 (Fig. 1C,D), for which good *in-vitro* evidence exists that they – or their highly conserved yeast orthologues – require the mammalian TRC or yeast GET pathway (Jonikas et al., 2009; Rivera-Monroy et al., 2016; Schuldiner et al., 2008; Stefanovic and Hegde, 2007; Stefer et al., 2011; Yamagata et al., 2010). Yet, the *in-vivo* reliance of these proteins on the pathway was reported to be variable or they turned out to be TRC40- and WRB-independent (Casson et al., 2017; Norlin et al., 2016; Rivera-Monroy et al., 2016). In HeLa cells, Sec61β, Sec22b, and Stx8 displayed reduced steady-state levels in the membrane fraction upon the combined down-regulation of *TRC40* and *WRB* (Fig. 1C,D). Interestingly, previous work reported proper localization of Sec61β in *TRC40*- or *WRB*-knockout cells or mouse tissue (Casson et al., 2017; Norlin et al., 2016; Rivera-Monroy et al., 2016) indicating that assays of subcellular localization may report less sensitively on an involvement of the TRC pathway than assessments of steady-state protein levels.

As a negative control for the assay, we included the TA-protein PTP1B, that is able to insert spontaneously into liposomes (Brambillasca et al., 2006), and squalene synthase (SQS) recently shown to be TRC40-independent (Guna et al., 2018; Shurtleff et al., 2018). For PTP1B no significant changes were observed upon silencing *TRC40* or both *WRB* and *TRC40* although the scatter of the observed signal does not exclude subtle effects (Fig. 1C,D). SQS steady-state levels increased upon combined knock-down of *TRC40* and *WRB*. The molecular mechanisms behind the steady-state levels of a protein may be complex. On the one hand, compensatory changes in other targeting pathways (Haßdenteufel et al., 2017) may hide TRC pathway dependence. On the other hand, effects downstream of *bona-fide* targeting substrates such as Stx5 may suggest targeting dependence of a complex partner whose stability is affected by the targeting client. Indeed, Sec22b is a SNARE partner protein of Stx5 (Hay et al., 1997) and its steady-state levels may be indirectly affected by the combined down-regulation of *WRB* and *TRC40*. For PTP1B and SQS, our results are consistent with the notion that they do not require the TRC pathway for proper targeting.

To avoid conclusions based on TA-protein steady-state levels alone, we developed a complementary approach to tackle the question whether a substrate displaying *in-vitro* dependence and *in-vivo* or *in-cellulo* independence of TRC40 *does use* the pathway when it is available. To more directly probe the propensity of a TA-protein precursor to be targeted by the TRC pathway, we were inspired by approaches from the protease, protein disulfide isomerase,

AAA ATPase, and GTPase fields that have used dominant negative forms of the respective enzyme to trap transiently interacting substrates (Chen et al., 2014; Flynn et al., 2003; Jessop et al., 2009; Klebe et al., 1995). Based on the current model of the TRC40 ATPase cycle and the associated conformations of the protein (Fig. 2A), we set out to address the flux through the TRC pathway by a substrate-trapping approach.

Expression of ATPase-impaired TRC40$_{D74E}$ alters the subcellular localization of TA-proteins

TRC40 and its yeast orthologue Get3 are members of the SIMIBI family of NTPases, which also includes the SRP (Bange and Sinning, 2013). In contrast to the GTPase activity of SRP, Get3 is an ATPase that undergoes large conformational changes in response to ATP binding and hydrolysis (Fig. 2A). Hence, several residues involved in ATP-binding or hydrolysis have been targeted to experimentally manipulate Get3. Several studies used Get3$_{G30R}$ (Johnson et al., 2013; Schuldiner et al., 2005; Shen et al., 2003; Suloway et al., 2009; Wang et al., 2011b), which targets the P-loop or Walker A motif and is predicted to be deficient in nucleotide-binding (Saraste et al., 1990). Another extensively used mutant is Get3$_{D57N}$, which targets the conserved Switch I ATPase domain. This mutation impairs the ATPase-activity of Get3 (Chio et al., 2017; Mateja et al., 2009; Stefer et al., 2011; Wang et al., 2011a) rather than abolishing nucleotide-binding. Based on the effects of changing the orthologous D45 in the Switch I domain of the bacterial homolog ArsA (Zhou and Rosen, 1999), we created Get3$_{D57E}$ (Powis et al., 2013), demonstrated its strongly impaired ATPase activity, and showed its inability to substitute for wild-type Get3 in yeast although the protein was well-expressed. The current model of the Get3 ATPase cycle and by extension TRC40 (Fig. 2A) predicts that a form of the protein that can bind but not hydrolyze ATP may capture but not release TA-protein substrates (Chio et al., 2017; Mariappan et al., 2011; Stefer et al., 2011). Our previous results with yeast Get3$_{D57E}$ (Powis et al., 2013), specifically the co-localization of Get3$_{D57E}$-GFP and a TA-protein substrate in intracellular foci, are consistent with the idea that TA-protein precursors may be trapped by this mutant in cells. To make use of this tool in the mammalian system where many more TA-proteins exist (Kalbfleisch et al., 2007), we constructed and characterized the homologous TRC40$_{D74E}$ mutant.

Originally, small TA-proteins such as Sec61β (Stefanovic and Hegde, 2007) or Ramp4 (Favaloro et al., 2008) were used as model substrates to identify the mammalian TRC pathway using an *in-vitro* membrane insertion assay and protein crosslinking. However, the SNARE

protein Stx5 is the best-characterized TRC40 substrate that critically depends on the presence of the pathway *in vivo* (Casson et al., 2017; Norlin et al., 2016; Norlin et al., 2018; Rivera-Monroy et al., 2016). Likewise, yeast syntaxin 5 (Sed5) requires Get3 for proper localization and targeting (Jonikas et al., 2009; Powis et al., 2013; Schuldiner et al., 2008; Voth et al., 2014). Therefore, we used Stx5 as a substrate to assess the impact of $TRC40_{D74E}$ on TA-protein insertion in an *in-vitro* insertion assay using a C-terminally opsin-tagged variant of the TA-protein substrate Stx5 (Fig. 2B). The opsin tag is an N-glycosylation tag that corresponds to 13 amino acids of bovine opsin. It becomes glycosylated on the luminal side once the protein is inserted into the ER. Thereby it enables to monitor the ER-insertion of the protein (Abell et al., 2007; Borgese et al., 2001; Favaloro et al., 2010; Honsho et al., 1998; Kutay et al., 1995; Masaki et al., 1996; Pedrazzini et al., 2000; Schuldiner et al., 2008; Stefanovic and Hegde, 2007). Reticulocyte lysate was immuno-depleted of TRC40, which strongly reduced glycosylation and hence insertion of Stx5 (Fig. 2B). Re-expressing either wild type TRC40 or $TRC40_{D74E}$ in the immuno-depleted lysate revealed that $TRC40_{D74E}$ was not capable of mediating the insertion of Stx5 (Fig. 2B). Instead, it was able to reduce the small amount of glycosylated and hence inserted Stx5 observed in the immuno-depleted sample.

In mammalian cells and in yeast, impairing the TRC/GET pathway leads to a loss of Stx5/Sed5 from the Golgi apparatus (Casson et al., 2017; Norlin et al., 2016; Rivera-Monroy et al., 2016; Schuldiner et al., 2008). Therefore, we used the subcellular localization of endogenous Stx5, determined by indirect immunofluorescence, as a readout to evaluate the effects of $TRC40_{D74E}$ over-expression (Fig. 2C). We transfected HeLa cells with c-Myc-tagged TRC40 constructs and performed double-labeling immunofluorescence staining for Stx5 and c-Myc-TRC40. Upon transfection with the $TRC40_{D74E}$ mutant, Stx5 changed its subcellular localization showing a diffuse, apparently cytoplasmic staining instead of the Golgi-staining that reflects proper membrane targeting and subsequent sorting of Stx5. Over-expression of $TRC40_{wt}$ showed a partially cytoplasmic staining for Stx5 (Fig. 2C) in line with the idea that the conformation stabilized by $TRC40_{D74E}$ reflects a step of the normal TRC40 cycle that can also be populated more by raising the TRC40 levels. Alternatively, over-expression of TRC40 may create a large pool of the ATPase free of TA-protein substrate. This form of TRC40 may titrate out the binding sites on the receptor required for proper Stx5 targeting. Using the $TRC40_{D74E}$-based assay, we revisited the TA-protein PTP1B, whose steady-state levels were not significantly affected by silencing the TRC pathway (Fig. 1C,D), and observed no obvious effects on its localization pattern (Fig. 2D).

To corroborate the trapping function of the Asp 74 to Glu mutant, we tested another presumably ATPase-deficient mutant, D74N, which was previously reported to constitutively bind TA-proteins in the background of Get3 (Mateja et al., 2009; Mateja et al., 2015; Stefer et al., 2011). Over-expression of TRC40$_{D74N}$ resulted in the same change of Stx5 subcellular localization (Fig. S1) that we had observed in the presence of TRC40$_{D74E}$ (Fig. 2C). This observation is in line with a recent report that TRC40$_{D74N}$ failed to restore proper distribution of Stx5 in dorsal pancreas explants (Norlin et al., 2018). We tested another *bona-fide* TRC40-substrate, EMD (Pfaff et al., 2016; Rivera-Monroy et al., 2016), and observed a diffusely distributed population when staining the TRC40$_{D74E}$-transfected cells for endogenous EMD (Fig. S2). Together, these results strengthen the notion that over-expression of TRC40 mutants, in which ATP-binding capacity is preserved but ATPase activity is impaired, may divert the TA-protein substrate from its subcellular destination, the Golgi membrane in the case of Stx5 or the inner nuclear membrane in the case of EMD.

Over-expression of TRC40$_{D74E}$ causes cytoplasmic accumulation of TA-proteins

In order to analyse whether the diffuse staining pattern observed for Stx5 and EMD in TRC40$_{D74E}$-transfected cells (Figs 2C, S2) reflected localization to the cytoplasm, we semi-permeabilized cells with digitonin before immunofluorescence staining (Fig. 3A). Digitonin preferentially permeabilizes the plasma membrane leaving the rest of the cell membranes intact (Plutner et al., 1992; Wilson et al., 1995). In untransfected cells, Stx5 was observed in its typical Golgi staining pattern (compare Fig. S3) upon digitonin semi-permeabilization but – as expected for cytoplasmic components – the diffuse Stx5 signal observed upon TRC40$_{D74E}$-transfection was washed out (Fig. 3B). This experiment indicates that Stx5 accumulates in the cytoplasm upon over-expression of TRC40$_{D74E}$.

To further corroborate this conclusion, we developed a stable cell line (Flp-In T-REx-293) with an opsin-tagged Stx5 at the C-terminus under the control of a tetracycline-inducible promoter. In order to biochemically investigate whether Stx5 is accumulated in the cytosol, as indicated by its cytoplasmic localization observed by immunofluorescence, we transfected the Stx5-opsin (Stx5-op) stable cell line with c-Myc-tagged TRC40 constructs before induction of the opsin-tagged substrate to create a pulse of Stx5 precursors. Next, we performed subcellular fractionation and analyzed the different fractions by Western blot. Stx5-op steady-state levels were higher in the cytosolic fraction of the cells transfected with TRC40$_{D74E}$ than in the those transfected with the empty vector (Fig. 3C), corroborating the observations obtained by microscopy. There was one strong band reflecting Stx5-op in the cytosolic as opposed to the

membrane fraction where we observed two (Fig. 3C). The single band observed in the cytosol is consistent with the interpretation that an unglycosylated biogenetic precursor was trapped. Furthermore, analysis of the membrane fraction suggested less Stx5-op was glycosylated and hence inserted into the membrane in the presence of over-expressed $TRC40_{D74E}$ as compared to $TRC40_{wt}$. These findings raise the possibility that $TRC40_{D74E}$ interacts with Stx5 in the cytoplasm and acts as a trap mutant impeding its handover to the TRC receptor to enable membrane-insertion.

Therefore, we tested whether $TRC40_{D74E}$ and endogenous Stx5 physically interact. We transfected HEK293 cells with c-Myc-TRC40 constructs and immuno-precipitated c-Myc-TRC40 from the cytosol in the absence of detergent, which was then probed for co-precipitating endogenous Stx5 (Fig. 3D). We also probed for Sec61β to test a candidate substrate that certainly *can* target via the TRC pathway as demonstrated by *in-vitro* assays (Favaloro et al., 2008; Favaloro et al., 2010; Stefanovic and Hegde, 2007), was affected in its steady-state levels upon TRC pathway silencing (Fig. 1C,D), but does not depend on it for proper subcellular localization (Casson et al., 2017; Rivera-Monroy et al., 2016). To corroborate our interpretation that $TRC40_{D74E}$ acts as a substrate trap, we introduced two additional mutations into the plasmid encoding the protein. These have been shown to reduce the affinity of the TA-binding groove – formed by the TRC40 dimer – for the TMS of the TA-protein (Mateja et al., 2009; Shao et al., 2017). The resulting c-Myc-$TRC40_{D74E/L190D/I193D}$ poorly co-precipitated Stx5 and Sec61β (Fig. 3D). Consistent with the notion that the diffuse Stx5 staining pattern in $TRC40_{D74E}$-transfected cells reflects a cytoplasmic population in complex with TRC40, the Golgi localization of Stx5 was partially rescued in the presence of the triple mutant $TRC40_{D74E/L190D/I193D}$ (Fig. S3). The effect of restoring the proper subcellular localization by combining the D74E mutation with the additional two mutations, which reduce the binding affinity of the TRC40 to the TMSs of TA-proteins, was very clear for EMD (Fig. S2). Thus, the cytosolic interaction, and hence the diffuse staining pattern observed for substrates in the presence of $TRC40_{D74E}$, correlated with an intact TA-binding groove consistent with our rationale to stabilize the TA-protein interacting form of TRC40. It should, however, be noted that much less is currently known about the molecular details of how Get3-like chaperones interact with their clients (Farkas et al., 2019; Voth et al., 2014). Hence, we cannot exclude that some of the effects of over-expressing $TRC40_{D74E}$ may not directly relate to membrane targeting of TA-protein precursors during biogenesis.

Characterization of TA-protein interactome of TRC40$_{D74E}$

Based on our characterization of TRC40$_{D74E}$ as a substrate trapping mutant, we applied this tool in two independent, complementary strategies to map the TRC40 client spectrum. On the one hand, we used a large panel of antibodies (Table S1) to test the presence of TA-proteins in the c-Myc-TRC40$_{D74E}$ immunoprecipitates (Fig. S4). As the silencing approach (Figs 1, S7), this approach is limited by the quality of the antibodies available. On the other hand, we conducted an unbiased mass spectrometry-based approach and transfected HEK293 cells with c-Myc-TRC40$_{D74E}$ and the corresponding triple mutant TRC40$_{D74E/L190D/I193D}$ that reduces the affinity of the TMS binding groove for TA-protein substrates (Fig. 3D). After subcellular fractionation and anti-c-Myc immuno-precipitation from the cytosol in the absence of detergent, the eluates were analyzed by unbiased label-free mass spectrometry. Qualitatively, 2329 proteins out of 3135 detected proteins were identified in either eluate, including 18 TA-proteins (Table S2). Since 95 TA-proteins were detected in whole-cell lysates of HEK293 cells (Geiger et al., 2012), we identified 20% of all robustly expressed TA-proteins in the cytosol of the transfected HEK293 cells. The eluates were then quantitatively compared by SWATH (Sequential Window Acquisition of All Theoretical Fragment Ion Spectra) (Lambert et al., 2013) mass spectrometry (Table S3 lists the peptides used for quantification). We corroborated the results corroborated by Western Blot analysis of individual c-Myc-TRC40 proteins and the amounts of co-immuno-precipitated Stx5 (Figs S4, S5). Both approaches unequivocally confirmed the results obtained in Figs 2 and 3, i.e. the trapping of Stx5 by TRC40$_{D74E}$, and hence the suitability of the approach to identify TA-proteins that *do* interact with TRC40.

The results of the SWATH mass spectrometry approach are depicted in a volcano plot of the enrichment with the single or triple TRC40 mutant plotted against the statistical significance of the result (Fig. 4). All components of the mammalian pretargeting complex, i.e. SGTA, BAG6, UBL4A, and TRC35 (magenta dots in Fig. 4) were detected in the eluates. Except for a possible modest enrichment of TRC35 with c-Myc-TRC40$_{D74E/L190D/I193D}$ these proteins showed no preference for either form of TRC40. With the exception of the golgin giantin, all TA-proteins (blue dots in Fig. 4, Table S2) were either present in equal amounts or enriched with c-Myc-TRC40$_{D74E}$. The positive control protein Stx5 was enriched about two-fold and right at the significance limit ($P < 0.05$). Focusing on the six TA-proteins that were enriched similarly or more strongly than Stx5 (Fig. 4, Table S2), i.e. UBE2J1, LAP2B, VAMP7, EMD, and VAPB (DCAKD was not studied further due to the unavailability of a specific antibody), we found all five to specifically co-immunoprecipitate with c-Myc-TRC40$_{D74E}$

(Table 1, Fig. S4A). As expected for EMD based on the literature (Pfaff et al., 2016) and the results presented here (Figs 1, S2), all five TA-proteins were confirmed as TRC40-interactors contacting the TA-binding groove (Fig. S4A).

The candidate-based approach using antibodies affords a much higher sensitivity for detecting TA-proteins in the TRC40-immunoprecipitaes. Using this strategy, we were able to substantially extend the number of tested TA-proteins. In addition to Stx5, Sec61β, and the five TA-proteins tested after identification by the SWATH mass spectrometry approach (EMD, VAPB, VAMP7, LAP2B, UBE2J1), we were able to obtain meaningful data regarding an additional 22 TA-proteins (Table 1, Fig. S4B,C). Importantly, this approach also revealed 7 TA-proteins that were not trapped by TRC40$_{D74E}$ although they were robustly detected in whole cell lysates (Fig. S4C). The total list of 30 probed TA-proteins is a valuable resource when corroborating or refuting rules that determine TRC40-dependence of a client.

We confirmed the capacity to create a diffuse, presumably cytoplasmic pool due to trapping by TRC40$_{D74E}$ for two additional syntaxins (Fig. S6). Stx6 is a SNARE protein involved in Golgi trafficking (Bock et al., 1996; Cheng et al., 2010) and has previously been implicated as a *bona-fide* TRC40 substrate with manipulation of the pathway *in vivo* affecting its steady-state levels and localization (Norlin et al., 2016; Rivera-Monroy et al., 2016). Stx8 is a SNARE protein localized at endosomes (Kasai et al., 2008; Prekeris et al., 1999; Subramaniam et al., 2000). Interestingly, its steady-state levels were not affected in the liver or the ventricle of the *Wrb* knockout mouse and its subcellular localization indicated robust membrane targeting (Rivera-Monroy et al., 2016). Although the two syntaxins reacted differently to the loss of the TRC pathway in these mouse tissues, they both enriched with TRC40$_{D74E}$ (Fig. S4B, Table 1). In line with this observation, we observed a partially diffuse staining pattern for endogenous Stx6 (Fig. S6A) and Stx8 (Fig. S6B) upon over-expression of the TRC40 trap. Many of the antibodies used for Western blotting were not suited for indirect immunofluorescence, which is why we limited ourselves to confirming the appearance of a presumably cytoplasmic pool for selected TA-proteins (Stx5, Stx6, Stx8, EMD). In all cases, physical interaction with TRC40$_{D74E}$ was predictive of the aberrant subcellular localization that is consistent with substrate trapping in the cytoplasm.

One TA-protein – the coiled-coil forming golgin giantin – was substantially enriched with the triple mutant c-Myc-TRC40$_{D74E/L190D/I193D}$ (Fig. 4). This behavior may suggest an interaction with TRC40 that does not depend on the TA-binding groove. Using an antibody against endogenous giantin, that worked well in indirect immunostaining but not Western blotting, we detected the protein in HeLa cells expressing wild type, the single, or the triple

mutant (Fig. 5A) and observed a diffuse and reduced Golgi staining pattern when either TRC40$_{D74E}$ or the triple mutant were expressed. Hence, giantin behaved similarly to Stx5 but, unlike it, did not react to the manipulation of the TA-binding groove. We hypothesized that the unusual presence of a histidine in the TMS of giantin (Fig. 5B) could explain the effect of the triple mutant on the subcellular localization of the protein. The exchange of two hydrophobic residues by aspartates creates a negative patch in the center of the TA-binding groove. Inspection of the TMS of other TA-golgins, i.e. golgin-84 and CASP (Gillingham and Munro, 2016), revealed a histidine in the same position (Fig. 5B). We tested whether they interacted with TRC40$_{D74E}$ or the triple mutant by immuno-precipitation (Fig. 5C,D). Indeed, golgin-84 and CASP interacted with both TRC40 variants or even preferred the triple mutant in the case of the golgin CASP.

To test whether this preference involved a charge interaction between the histidine and the negatively charged TMS binding groove, we introduced positively charged side chains and created the triple mutant c-Myc-TRC40$_{D74E/L190K/I193K}$, which should make binding of an TMS containing a histidine energetically unfavorable. In the case of golgin-84 but not CASP, this reduced the interaction substantially with respect to co-purification with TRC40$_{D74E}$ or the negatively charged triple mutant (Fig. 5C,D). With respect to golgin-84, our result confirms a report by Casson et al. (2017) who also described an interaction of the protein with TRC40 (without testing its dependence TMS-binding groove) but observed no effect on its steady-state localization in a TRC40 knock-out cell line (Casson et al., 2017). In summary, we conclude from our data that the TA-golgins fall into the class of substrates that *can* be targeted by the TRC pathway but do not absolutely require it for correct subcellular localization (Casson et al., 2017). Interestingly, we observed strong reductions in the steady-state levels of both CASP and golgin-84 upon combined silencing of *WRB* and *TRC40* (Fig. S7) further corroborating the notion that the TRC pathway is highly relevant to their turnover. While our results plausibly support a model where TRC40 can target the TA-protein golgins they also highlight that a proportion of the observed TRC40-co-purifying pool may reflect an interaction in a functional context distinct from precursor targeting. Given the important roles of Stx5, Stx6, and the golgins in Golgi morphology and function more work will be required to determine how direct and indirect effects combine to result in the observed reduction at the steady-state.

Figure 6 summarizes the data for the whole TA-protein panel that we investigated in experiments probing the enrichment by the TRC40$_{D74E}$ mutant (Fig. 6A based on data in Figs 3, 4, S4, S5 and Table 1) or TA-protein steady-state levels upon combined *TRC40* and *WRB* silencing (Fig. 6B based on data in Figs 1, S7) plotted against the hydrophobicity of the

respective TMS. A dotted line indicates the hydrophobicity score of the Sec61β TMS previously proposed as the dividing line that determines TRC40-dependence of a TA-protein precursor (Guna et al., 2018). We chose the GRAVY score (Kyte and Doolittle, 1982) instead of the transmembrane tendency score (Zhao and London, 2006) to describe the properties of the TMSs. The main difference between the two scores lies in the weight allocated to aromatic residues, which frequently occur in membrane proteins but are less hydrophobic than aliphatic side chains. However, no systematic differences were observed when correlating our experimental results with the series of TMS scores determined by one or the other method.

While both experimental parameters generally correlate well with TMS hydrophobicity, i.e. most TA-proteins with a TMS more hydrophobic than Sec61β *do* interact with TRC40 and respond to the manipulation of the TRC pathway, the dividing line defines a region of TMS hydrophobicity where it is impossible to predict whether a TA-protein is affected by the trap or the silencing. In fact, our data provide examples of proteins that interacted but whose steady-state levels were not affected (Stx18, GOSR2) or vice versa (Fis1, MOSPD2). Furthermore, we found TA-proteins with TMSs in a hydrophobicity range identical to *bona-fide* substrates (SYNE1, SYNE3, ZFPL1; red dots in Fig. 6A based on Fig. S4C) that we were unable to trap using $TRC40_{D74E}$ although their steady-state levels were strongly affected when the TRC pathway was not operational. In conclusion and after careful consideration of the caveats associated with either experimental strategy, the data presented in Fig. 6 allow a reassessment of the properties of a TA-protein relevant to its interaction with TRC40, which may represent a combination of interactions during biogenesis including membrane targeting and other functional contexts.

Discussion

In vitro approaches have been extensively used to study the functional interaction of TRC40 with different TA-proteins (Favaloro et al., 2008; Favaloro et al., 2010; Johnson et al., 2012; Leznicki et al., 2010; Leznicki et al., 2011; Mariappan et al., 2011; Rabu et al., 2008; Stefanovic and Hegde, 2007). The hydrophobicity of the TMS has been considered a key factor for organelle targeting (Borgese et al., 2001; Borgese et al., 2003; Borgese et al., 2007; Bulbarelli et al., 2002) as well as for discriminating between different targeting pathways to the same subcellular compartment (Costello et al., 2017b; Guna and Hegde, 2018; Guna et al., 2018; Rabu et al., 2008; Rabu et al., 2009; Yagita et al., 2013). The diversity of the targeting

pathways raises the question which pathway is in charge of the biogenesis of a given TA-protein when all pathways are operational.

In order to address this problem, we developed an ATPase-impaired, dominant-negative mutant of TRC40 that is able to trap TA-proteins in the cytoplasm. For the first time, it has been possible to co-immunoprecipitate TRC40, preserving the interactions with endogenous TA-proteins, without the use of crosslinkers. This tool enables us to identify the *in-vivo* TA-protein interactome of TRC40 in human cells (Fig. 6A). We used both, candidate testing as well as unbiased identification of the most enriched targeting clients. We identified novel TRC40 targets, such as VAPA and VAPB, which are involved in membrane contact sites and lipid exchange between organelles (Costello et al., 2017a; Dong et al., 2016; Hua et al., 2017; Manford et al., 2012; Rocha et al., 2009), and the subclass of coiled-coil forming golgins, such as giantin, golgin-84, and CASP, that are tethered to the medial Golgi by a C-terminal TMS. Although the interpretation of the TRC40 interaction that we observed in terms of biogenesis is consistent with all experimental evidence and the current model of TRC40-dependent targeting we cannot exclude that the trapped intermediates may also reflect an intermediate of another TRC40-related pathway, i.e. in the context of cellular quality control or proteostasis. In fact, the interaction of $TRC40_{D74E}$ with the TA-protein golgin CASP did not depend on an intact hydrophobic groove thought to accommodate the TMS of TA-proteins (Fig. 5 C,D) suggesting that TRC40 may recognize another aspect of this golgin.

In line with the proposed cut-off for TRC40 interaction (Guna et al., 2018), we have trapped one TA-protein with a TMS hydrophobicity score substantially lower than that of Sec61β, i.e. Stx18 (1.62 versus 2.05) based on the GRAVY score to determine TMS hydrophobicity (Kyte and Doolittle, 1982). However, using transmembrane tendency (Zhao and London, 2006) the TMS of Sec61β and Stx18 score similarly (21.45 versus 21.62). Generally, this does not mean that transmembrane tendency is a better predictor of the ability of a TA-protein to interact with TRC40 since the UBE2J1 and GOSR2 TMS score substantially lower than Sec61β using transmembrane tendency but were nevertheless trapped (this was better predicted by the GRAVY score where they show a higher hydrophobicity than Sec61β, Fig. 6A). As expected based on the hydrophobicity of the TMS by either score, we exclude PTP1B as a TRC40 client: Only marginal effects on its steady-state levels were observed upon combined *WRB* and *TRC40* silencing and it did not co-immunoprecipitate with the trapping mutant of TRC40 although it was well detected in the cell lysates. This is consistent with the finding that PTP1B was able to spontaneously insert into liposomes (Brambillasca et al., 2006). The two mitochondrial proteins investigated, BNIP3L and Fis1, were not enriched with the trap

mutant (Fig. S4B,C). However, their steady-state levels reacted differently to the combined silencing of *TRC40* and *WRB*: This manipulation strongly reduced the steady-state levels of Fis1 but not BNIP3L (Fig. S7). Taken together, these results are consistent with the notion that mitochondrial TA-proteins do not use the TRC pathway (Figueiredo Costa et al., 2018). Hence, the effect on Fis1 steady-state levels may relate to another function of TRC40.

We identified three TA-proteins, SYNE1, SYNE3, and ZFPL1 that were not trapped by $TRC40_{D74E}$ (Figs S4C, 6A) despite a TMS hydrophobicity score that would have predicted an interaction with TRC40 during biogenesis. We cannot exclude that such a failure to be trapped may reflect a low amount of TA-protein precursor present in the cell although ZFPL1 was abundantly detected in HeLa and HEK293 cells (Cho et al., 2018; Geiger et al., 2012). Generally, we found no indication that copy numbers or half-life – as available from systematic studies on protein turnover in HeLa cells (Cambridge et al., 2011; Cho et al., 2018) – correlated with the propensity of a TA-protein to be trapped by $TRC40_{D74E}$. For example, TA-proteins identified by SWATH mass spectrometry with high confidence ranged from 140 million molecules per cell and a half-life of 47 hours (EMD) to 3 million and 20 hours (Stx5) or even only 800 thousand molecules per cell (UBE2J1). In fact, based on the available data (Cambridge et al., 2011; Cho et al., 2018) VAPB (80 million molecules per cell and 42 h) and FIS1 (56 million and 40 h) or GOSR2 (10 million, 29 h) and PTP1B (6 million, 31 h) are pairs of TA-proteins of very similar abundance and half-life that perfectly underscore TMS hydrophobicity as the dominant parameter as a prediction for TRC40 recruitment in live cells.

The TRC40 triple mutant we generated disturbs the hydrophobic pocket of TRC40. Consistent with the expectation that this manipulation would reduce the affinity of $TRC40_{D74E}$ for TA-proteins we observed a strong reduction in co-immunoprecipitation of most TA-protein substrates (Figs 3D, 4, S4, S5). However, the two TA-golgins golgin-84 and CASP were clear exceptions as they co-purified equally or even more strongly with the triple mutant compared to $TRC40_{D74E}$. We attribute this to a central histidine within the TMS of the TA-golgins that may be able to interact electrostatically with the mutant, now negatively charged, binding pocket of TRC40. Consistent with this notion, golgin-84 interacted substantially less with a charged-inverted triple mutant $TRC40_{D74E/L190K/I193K}$. In contrast, CASP co-purified more extensively with either triple mutant compared to $TRC40_{D74E}$. This suggests that the interaction between TRC40 and CASP is independent of the TA-binding groove and may instead be based on TRC40's chaperone activity.

The yeast GET pathway is encoded by non-essential genes (Schuldiner et al., 2008) despite the fact that a strongly Get3-dependent substrate, i.e. Sed5 (yeast Stx5), is encoded by an essential gene (Giaever et al., 2002). The phenotypes of *get* deletion mutants become apparent under stress conditions such as heat or oxidative stress (Kiktev et al., 2012; Metz et al., 2006). In contrast, the TRC pathway is essential in mammalian cells (Mukhopadhyay et al., 2006; Tran et al., 2003). The identification of novel TA-protein substrates presented here provides new avenues into understanding why this system is so important in multicellular organisms: VAPA, encoded by a gene essential for early embryonic development in the mouse (McCune et al., 2017), and VAPB are important for membrane contacts and lipid homeostasis (Costello et al., 2017a; De Vos et al., 2012; Hua et al., 2017). The TA-protein subgroup of golgins plays a major role in organizing vesicular traffic between the different cisternae of the Golgi (reviewed in Munro, 2011). They are key determinants of the posttranslational modification of secretory proteins in the Golgi. In particular, giantin is required for the proper localization and activity of Golgi-resident glycosyltransferases (Stevenson et al., 2017). Together with SNARE proteins – active in the Golgi and the endosomal pathway – the client spectrum of the TRC pathway suggests a scope that will not only affect the trafficking, but also the posttranslational modification of secretory proteins, and the homeostasis of the endomembrane system at large.

Our findings offer a satisfying synthesis of information on TA-protein targeting obtained by different approaches (Fig. 7). Even though redundant with other targeting options, the TRC pathway represents a robust route to the ER and accommodates a large client spectrum (Fig. 7 group 1). The precise flux may differ from cell type to cell type: While Stx8 steady-state levels were not affected in a *Wrb*-knockout mouse model (Rivera-Monroy et al., 2016) the protein was reduced in HeLa cells upon silencing of *TRC40* and *WRB* (Figs 1, 6B). For some clients the TRC pathway may be nothing but a back-up option (group 2). In several cases TRC pathway manipulation affected the steady-state levels of proteins (Fig. 7 group 3) but no interaction with the TRC40 trap was observed. The explanation may differ for the different TA-proteins in this group, ranging from indirect effects to a very low rate of biogenesis. Some of the TA-proteins in this group feature a TMS hydrophobicity score well compatible with TRC40-dependent targeting (the nesprins SYNE1 and SYNE3 and ZFPL1) and it will be interesting to obtain further insights into their biogenesis.

An important dimension that is rarely studied in the context of targeting experiments is the functional outcome of targeting by different pathways for individual proteins. After biogenesis and to fulfill their cellular functions, the golgins, Stx5, and the VAPs all undergo many diverse and often reversible protein-protein interactions resulting in coiled-coils, SNARE bundles, or dynamic tethers between two membranes. Since a chaperone holdase activity of Get3 has been reported (Voth et al., 2014), it may be worth considering that the TRC pathway could aid its clients beyond targeting by chaperoning their cytoplasmic domains. In the case of Stx5, we have provided some evidence that critical determinants of TRC40-dependence may map to the N-terminal domain of the TA-protein (Rivera-Monroy et al., 2016). So far, all analyses demonstrating proper targeting of a TA-protein in the absence of the TRC pathway conclude that targeting was covered by another pathway, because no effect on the steady-state levels or localization of the protein was observed. However, the functionality of TA-proteins that can be targeted by TRC40 but do not strictly require it has never been explored, namely with respect to the protein-protein interactions of their N-terminal domains or their dynamic behavior within the membrane. We propose that a full understanding of TA-protein targeting will eventually include mechanisms that cater to the function of specific TA-proteins in addition to ensuring that they are brought to the right membrane during the initial phase of biogenesis.

Materials and Methods

Plasmids and constructs

All constructs were obtained using standard molecular biology methods and all sequences were verified by Sanger sequencing (GATC Biotech, Konstanz, Baden-Württemberg, Germany).

pcDNA3.1(-)_c-Myc-TRC40 was obtained after subcloning it from MBP-TEV-TRC40/ZZ-EMD-opsin, previously described (Favaloro et al., 2010), into a pcDNA3.1(-) (Invitrogen, Carlsbad, CA, USA) by using overlap extension PCR. Primers for mutagenesis of TRC40 contained a sequence for making it insensitive to the small interference RNA (Catalog#: s1675; Ambion, Austin, TX, USA) that was described before (Pfaff et al., 2016; Rivera-Monroy et al., 2016). First, one PCR using a forward primer containing an N-terminal c-Myc-tag for TRC40 and a restriction site for XhoI (ATACTACTCGAGATGGAGCAGAAACTCATCTCTGAAGAGGATCTGATGGCGGCAGGGGTGGCC) and the reverse primer (TTGGGAAATAAAGGGGGAGATCTGGTTCTTGATCTGCAT) contained the sequence to

be mutagenized. Second, another PCR using a forward primer (TCCCCCTTTATTTCCCAAATGTGCAACATGCTGGGCCTGG), overlapping the sequence of the aforementioned reverse, and a reverse primer targeting the C-terminus of TRC40 and containing a restriction site for BamHI (ATACTAGGATCCCTACTGGGCACTGGGGGGCT) was performed. A third PCR using the products of the first two PCRs was performed. The PCR-product was cloned into pcDNA3.1(-) using BamHI and XhoI.

The pcDNA3.1(-)_c-Myc-TRC40 mutants were obtained by site-directed mutagenesis using the following primers: D74E forward primer (GTGTTCTGATCATCTCCACAGAGCCAGCACACAACATCTCAG) and reverse primer (CTGAGATGTTGTGTGCTGGCTCTGTGGAGATGATCAGAACAC); D74N forward primer (GTGTTCTGATCATCTCCACAAACCCAGCACACAACATCTCAG) and reverse primer (CTGAGATGTTGTGTGCTGGGTTTGTGGAGATGATCAGAACAC); I193D forward primer (CCTGGGCCGGCTTATGCAGGACAAGAACCAGATCTCC) and reverse primer (GGAGATCTGGTTCTTGTCCTGCATAAGCCGGCCCAGG); L190D/I193D forward primer (GGAGCGGGGCCTGGGCCGGGACATGCAGGACAAGAACCAG) and reverse primer (CTGGTTCTTGTCCTGCATGTCCCGGCCCAGGCCCCGCTCC); L190K/I193K forward primer (CGTGGAGCGGGGCCTGGGCCGGAAGATGCAGAAGAAGAACCAGATCTCCCCCTTTATTTCC) and reverse primer (GGAAATAAAGGGGGAGATCTGGTTCTTCTTCTGCATCTTCCGGCCCAGGCCCCGCTCCACG).

The plasmid pGEM3Z-Stx5-opsin for the *in vitro* transcription and translation assays was described before (Rivera-Monroy et al., 2016). For pET23b_c-Myc-TRC40 constructs pcDNA3.1(-)_c-Myc-TRC40 plasmids were digested with NheI and HindIII and the inserts were ligated into a pET23b.

Cell culture

HeLa P4 cells (Charneau et al., 1994) were obtained from the NIH AIDS Reagent Program. HeLa P4 and T-REx 293 Stx5-op cells were grown in DMEM (Gibco, Carlsbad, CA, USA) supplemented with 2 mM L-glutamine (Gibco) and 10% (v/v) FBS (Biochrom, Berlin, Germany) in a 37°C incubator at 5% CO_2. They were tested for contamination by *Mycoplasma* spp. on a regular basis.

T-REx 293 Stx5-opsin cell line generation

Flp-In T-REx 293 cells (Invitrogen) were cultured with DMEM supplemented with 10 µg/mL blasticidin. pOG44 and pcDNA5/FRT/TO_Stx5-opsin plasmids, described previously, were co-transfected. Two days after transfection, cells were selected by incubating with DMEM++ supplemented with 15 µg/mL blasticidin and 200 µg/mL hygromycin B for two weeks until obtaining positive clones. The expression of Stx5-op from the stable transfectants was tested by Western blot. For inducing the expression of Stx5-op, 1 µg/mL tetracycline was added into the medium and the cells were incubated at 37°C for 6 h.

Cell transfection and knockdown

HeLa P4 or T-REx 293 cells were seeded to be 60-80% the day of transfection. Lipofectamine 2000 (Invitrogen) was used for transfections. Cell were incubated for 6 h and then harvested 48 h after Lipofectamine 2000 transfection.

Small interference RNA (siRNA) was used for the knockdown of *TRC40* and *WRB*. Specific RNA oligos against WRB and TRC40 were described previously (Rivera-Monroy et al., 2016) and luciferase siRNA (sense: CGUACGCGGAAUACUUCGA, antisense: UCGAAGUAUUCCGCGUACG, Sigma-Aldrich) was used as control. For the knockdown, cells were transfected twice at 48 h interval using Lipofectamine RNAiMAX (Invitrogen). Cells were incubated for 24 h with the RNAiMAX-siRNA solution and harvested 48 h after the last transfection.

Cell fractionation

The lysis of the cells was performed with a dounce homogenizer and the lysate was centrifuged for 1 h at 180,000 *g* at 4°C for sedimenting the membranes. The pellet was resuspended and centrifuged again at 180,000 *g* for 20 min at 4°C. The cytosolic and membrane fractions underwent protein extraction with solubilization buffer, as previously described (Kline et al., 2009). Finally, cytosolic and membrane fractions were subjected to TCA precipitation, and proteins later resuspended in SDS loading buffer.

Indirect immunofluorescence

Cells were grown in coverslips, fixed with 4% (w/v) paraformaldehyde (PFA) in PBS for 15 min and then permeabilized with 0.05% SDS in PBS/0.3% Triton X-100 for 10 min at room temperature. Cells were blocked in 10% FBS in PBS for 30 min and incubated with primary antibodies diluted in 5% FBS in PBS overnight at 4°C. Incubation with Alexa Fluor secondary antibodies (Invitrogen) was performed for 60 min at room temperature. The samples were mounted with Mowiol-DAPI. The list of antibodies can be found in Table S1. Cells were analyzed using an Axiovert 200M fluorescence microscope with a 63× Plan-Neofluar 1.3 NA water-corrected objective and appropriate filter settings. Images were acquired by using a LSM 510-META confocal laser scanning microscope (Zeiss, Jena, Thuringia, Germany). For confocal imaging a UV laser (405 nm) at 25 mW, a tunable Argon laser (488 nm) at 30 mW, HeNe laser line (543 nm) at 1 mW, HeNe laser lines (633 nm) at 3 mW were used for excitation. Emission filters: 450/60 nm, 518/25 nm, 588/56 nm, long-pass (LP) 650 nm respectively. The analysis of the images was performed with ImageJ 1.51w software (US National Institutes of Health, Bethesda, USA) (Schneider et al., 2012).

Digitonin semipermeabilization

HeLa P4 cells on coverslips were semi-permeabilized with a solution of 0.007% of digitonin in transport buffer (20 mM HEPES, 110 mM KOAc, 2 mM $Mg(OAc)_2$, 1 mM EGTA, pH 7.3, 2 mM DTT, 0.1 mM PMSF and 1 µg/ml each of leupeptin, pepstatin and aprotinin) for 5 minutes on ice in living cells prior to fixation. Control cells were permeabilized with 0.3% Triton X-100/0.05% SDS in PBS after PFA fixation.

TRC40 co-immunoprecipitation

Cells expressing empty vector (EV), wt, D74E, D74E/L190D/I193D, D74E/L190K/I193K c-Myc-TRC40 variants from 15 cm dishes were polytron-homogenized in 500 µL IP buffer (50 mM HEPES, 150 mM NaCl, 1.5 mM $MgCl_2$, 1 mM EGTA, pH 7.4). 2.5 mg of total lysate was diluted with IP buffer to 1.2 mL and centrifuged at 180,000 *g* for 1 h to obtain the cytosolic fraction.

200 µL of cytosol were used as input. The rest, approximately 1 mL, was incubated for 2.5 h in a rotation wheel with 50 µL Pierce Anti-c-Myc agarose resin (Thermo Scientific, Waltham, MA, USA) previously blocked with 5% BSA in IP buffer for 1 h. The resin was transferred to

600 µL columns and washed 3 times (2 min each) prior elution with 50 µL 1x loading buffer plus 100 mM DTT.

Mass spectrometric analysis

Samples were reconstituted in 1× NuPAGE LDS Sample Buffer (Invitrogen) and applied to 4-12 % NuPAGE Novex Bis-Tris Minigels (Invitrogen). For quantitation, samples were run 1 cm into the gel for purification. For generation of a spectral library, pooled aliquots of biological replicates for each sample were run half-distance through the gel. Gels were stained with Coomassie Blue for visualization purposes, and the library lanes cut into 12 equidistant slices regardless of staining. Quantitation samples were processed as a single slice. After washing, gel slices were reduced with dithiothreitol (DTT), alkylated with 2-iodoacetamide and digested with trypsin overnight. The resulting peptide mixtures were then extracted, dried in a SpeedVac, reconstituted in 2% acetonitrile/0.1% formic acid/ (v:v) and prepared for nanoLC-MS/MS as described previously (Atanassov and Urlaub, 2013). All samples were spiked with a synthetic peptide standard used for retention time alignment (iRT Standard, Biognosys, Schlieren, Switzerland).

Protein digests were analyzed on a nanoflow chromatography system (Eksigent nanoLC425) hyphenated to a hybrid triple quadrupole-TOF mass spectrometer (TripleTOF 5600+) equipped with a Nanospray III ion source (Ionspray Voltage 2400 V, Interface Heater Temperature 150°C, Sheath Gas Setting 12) and controlled by Analyst TF 1.7.1 software build 1163 (all Sciex, Framingham, MA, USA). In brief, peptides were dissolved in loading buffer (2% acetonitrile, 0.1% formic acid in water) to a concentration of 0.3 µg/µl. For each analysis 1.5 µg of digested protein were enriched on a precolumn (0.18 mm ID x 20 mm, Symmetry C18, 5 µm; Waters, Milford/MA, USA) and separated on an analytical RP-C18 column (0.075 mm ID x 250 mm, HSS T3, 1.8 µm, Waters) using a 55 min linear gradient of 5-35 % acetonitrile/0.1% formic acid (v:v) at 300 nl min^{-1}.

Qualitative LC/MS/MS analysis was performed using a Top25 data-dependent acquisition method with an MS survey scan of *m/z* 350–1250 accumulated for 350 ms at a resolution of 30,000 full width at half maximum (FWHM). MS/MS scans of *m/z* 180–1600 were accumulated for 100 ms at a resolution of 17,500 FWHM and a precursor isolation width of 0.7 FWHM, resulting in a total cycle time of 2.9 s. Precursors above a threshold MS intensity of 125 cps with charge states 2+, 3+, and 4+ were selected for MS/MS, the dynamic exclusion time was set to 30 s. MS/MS activation was achieved by CID using nitrogen as a collision gas and the

manufacturer's default rolling collision energy settings. One technical replicate per gel slice was analyzed to construct a spectral library.

For quantitative SWATH analysis, MS/MS data were acquired using 65 variable size windows (Zhang et al., 2015) across the 400-1,050 *m/z* range. Fragments were produced using rolling collision energy settings for charge state 2+, and fragments acquired over an *m/z* range of 350–1400 for 40 ms per segment. Including a 100 ms survey scan this resulted in an overall cycle time of 2.75 s. 3x3 replicates were acquired for each biological state for quantitation purposes. Protein identification was achieved using ProteinPilot Software version 5.0 build 4769 (AB Sciex) at "thorough" settings. A total of 541,419 MS/MS spectra from the combined qualitative analyses were searched against the UniProtKB human reference proteome (revision 04-2018, 93,609 entries) augmented with a set of 52 known common laboratory contaminants to identify 3,135 proteins at a False Discovery Rate (FDR) of 1%.

Spectral library generation and SWATH peak extraction were achieved in PeakView Software version 2.1 build 11041 (Sciex) using the SWATH quantitation microApp version 2.0 build 2003. Following retention time correction using the iRT standard, peak areas were extracted using information from the MS/MS library at an FDR of 1% (Lambert et al., 2013). The resulting peak areas were then summed to peptide and finally to 2,329 protein area values across all injections, which were used for further statistical analysis.

Western-blot

Antibodies were diluted in blocking buffer: 5% milk in PBS plus 0.1% Tween-20. The list of primary and secondary antibodies can be found in Table S1. The opsin monoclonal antibody (R2-15) was obtained from the laboratory of Bernhard Dobberstein from the University of Heidelberg and it was a kind gift from Paul A. Hargrave from the University of Florida that was described before (Adamus et al., 1991). TRC40 #4 and Sec61β antibodies were a kind gift from the laboratory of Bernhard Dobberstein. BAG6 antibody was a kind gift from the laboratory of Stephen High. Blots were scanned using an Odyssey CLx infrared scanner (LI-COR Biosciences, Lincoln, NE, USA) with IRDye LI-COR secondary antibodies (Table S1). The acquired images were analyzed and quantified with Image Studio 5.2.5 software (LI-COR).

Coupled in vitro transcription and translation

Reactions were performed in the TnT Quick Coupled Transcription/Translation System (Promega, Madison, WI, USA) on TRC40-immunodepleted reticulocyte lysate (using rabbit anti-TRC40 #4) or rabbit IgG-treated lysate as control (Johnson et al., 2012; Leznicki et al.,

2010; Pfaff et al., 2016). First, 150 ng of pET23b_c-Myc-TRC40 variants were added to 4.5 µL of each lysate and incubated for 30 min at 30°C (reaction #1). In the meantime, 250 ng of pGEM3Z_Stx5-op were added to a second set of 4.5 µL aliquoted lysates and kept on ice until use (reaction #2). Second, reactions #1 and #2 were combined and the transcription/translation was carried out for additional 90 minutes at 30°C. Third, the ER-integration assay was performed by adding 1 µL of pancreatic rough microsomes (RM) to the reaction mix and incubating it for 90 min at 30°C. Finally, the assay was stopped with 30 µL SDS-sample buffer at 55°C and Western blot analysis was performed for TRC40 and Stx5-op with 25% of the sample.

Statistics

Data are presented as mean±s.e.m. Statistical analysis was assessed via an unpaired parametric two-tailed Student's *t*-test. To determine statistical significance ($P<0.05$) GraphPad Prism 6.0 (GraphPad Prism Inc., San Diego, CA, USA) was used.

Acknowledgements

This study was partially supported by a grant of the People Programme (Marie Curie Actions) of the European Union's Seventh framework Programme FP7/2007-2013/ under REA grant agreement n° [607072] to B. Schwappach and J. Coy-Vergara. J. Coy-Vergara and J. Rivera-Monroy were also funded by the Deutsche Forschungsgemeinschaft within SFB 1002 (TP A07 led by B. Schwappach). Mass spectrometry was supported by SFB 1190 (TP Z02 led by H. Urlaub and C. Lenz). We are grateful to N. Borgese, M. Schuldiner, and several Schwappach lab members for helpful discussions and comments on the manuscript.

Author contributions

J.C.V., J.R.M. and B.S. designed research; J.C.V., J.R.M. and C.L. performed research; J.C.V., J.R.M., C.L., H.U., and B.S. analyzed data; J.C.V. and B.S. wrote the manuscript; all authors revised the manuscript.

References

Abell, B. M., Pool, M. R., Schlenker, O., Sinning, I. and High, S. (2004). Signal recognition particle mediates post-translational targeting in eukaryotes. *EMBO J.* **23**, 2755–64.

Abell, B. M., Rabu, C., Leznicki, P., Young, J. C. and High, S. (2007). Post-translational integration of tail-anchored proteins is facilitated by defined molecular chaperones. *J. Cell Sci.* **120**, 1743–1751.

Adamus, G., Zam, Z. S., Arendt, A., Palczewski, K., McDowell, J. H. and Hargrave, P. A. (1991). Anti-rhodopsin monoclonal antibodies of defined specificity: characterization and application. *Vision Res.* **31**, 17–31.

Atanassov, I. and Urlaub, H. (2013). Increased proteome coverage by combining PAGE and peptide isoelectric focusing: comparative study of gel-based separation approaches. *Proteomics* **13**, 2947–55.

Aviram, N., Ast, T., Costa, E. A., Arakel, E. C., Chuartzman, S. G., Jan, C. H., Haßdenteufel, S., Dudek, J., Jung, M., Schorr, S., et al. (2016). The SND proteins constitute an alternative targeting route to the endoplasmic reticulum. *Nature* **540**, 134–138.

Bange, G. and Sinning, I. (2013). SIMIBI twins in protein targeting and localization. *Nat. Struct. Mol. Biol.* **20**, 776–80.

Bock, J. B., Lin, R. C. and Scheller, R. H. (1996). A new syntaxin family member implicated in targeting of intracellular transport vesicles. *J. Biol. Chem.* **271**, 17961–5.

Borgese, N., Gazzoni, I., Barberi, M., Colombo, S. and Pedrazzini, E. (2001). Targeting of a tail-anchored protein to endoplasmic reticulum and mitochondrial outer membrane by independent but competing pathways. *Mol. Biol. Cell* **12**, 2482–96.

Borgese, N., Colombo, S. and Pedrazzini, E. (2003). The tale of tail-anchored proteins: coming from the cytosol and looking for a membrane. *J. Cell Biol.* **161**, 1013–9.

Borgese, N., Brambillasca, S. and Colombo, S. (2007). How tails guide tail-anchored proteins to their destinations. *Curr. Opin. Cell Biol.* **19**, 368–375.

Bozkurt, G., Stjepanovic, G., Vilardi, F., Amlacher, S., Wild, K., Bange, G., Favaloro, V., Rippe, K., Hurt, E., Dobberstein, B., et al. (2009). Structural insights into tail-anchored protein binding and membrane insertion by Get3. *Proc. Natl. Acad. Sci. U. S. A.* **106**, 21131–6.

Brambillasca, S., Yabal, M., Makarow, M. and Borgese, N. (2006). Unassisted translocation of large polypeptide domains across phospholipid bilayers. *J. Cell Biol.* **175**, 767–77.

Bulbarelli, A., Sprocati, T., Barberi, M., Pedrazzini, E. and Borgese, N. (2002). Trafficking of tail-anchored proteins: transport from the endoplasmic reticulum to the plasma membrane and sorting between surface domains in polarised epithelial cells. *J. Cell Sci.* **115**, 1689–702.

Cambridge, S. B., Gnad, F., Nguyen, C., Bermejo, J. L., Krüger, M. and Mann, M. (2011). Systems-wide proteomic analysis in mammalian cells reveals conserved, functional protein turnover. *J. Proteome Res.* **10**, 5275–5284.

Casson, J., McKenna, M., Haßdenteufel, S., Aviram, N., Zimmerman, R. and High, S. (2017). Multiple pathways facilitate the biogenesis of mammalian tail-anchored proteins. *J. Cell Sci.* **130**, 3851–3861.

Charneau, P., Mirambeau, G., Roux, P., Paulous, S., Buc, H. and Clavel, F. (1994). HIV-1 reverse transcription. A termination step at the center of the genome. *J. Mol. Biol.* **241**, 651–62.

Chen, Y.-C., Umanah, G. K. E., Dephoure, N., Andrabi, S. a, Gygi, S. P., Dawson, T. M., Dawson, V. L. and Rutter, J. (2014). Msp1/ATAD1 maintains mitochondrial function by facilitating the degradation of mislocalized tail-anchored proteins. *EMBO J.* **33**, 1548–64.

Cheng, J., Cebotaru, V., Cebotaru, L. and Guggino, W. B. (2010). Syntaxin 6 and CAL mediate the degradation of the cystic fibrosis transmembrane conductance regulator. *Mol. Biol. Cell* **21**, 1178–87.

Chio, U. S., Chung, S., Weiss, S. and Shan, S. (2017). A protean clamp guides membrane targeting of tail-anchored proteins. *Proc. Natl. Acad. Sci. U. S. A.* **114**, E8585–E8594.

Cho, H., Chio, U. S. and Shan, S.-O. (2018). In vitro Assays for Targeting and Insertion of Tail-Anchored Proteins Into the ER Membrane. *Curr. Protoc. cell Biol.* **81**, e63.

Costello, J. L., Castro, I. G., Hacker, C., Schrader, T. A., Metz, J., Zeuschner, D., Azadi, A. S., Godinho, L. F., Costina, V., Findeisen, P., et al. (2017a). ACBD5 and VAPB mediate membrane associations between peroxisomes and the ER. *J. Cell Biol.* 1–12.

Costello, J. L., Castro, I. G., Camões, F., Schrader, T. A., McNeall, D., Yang, J., Giannopoulou, E.-A., Gomes, S., Pogenberg, V., Bonekamp, N. A., et al. (2017b). Predicting the targeting of tail-anchored proteins to subcellular compartments in mammalian cells. *J. Cell Sci.* **130**, 1675–1687.

De Vos, K. J., Mórotz, G. M., Stoica, R., Tudor, E. L., Lau, K.-F., Ackerley, S., Warley, A., Shaw, C. E. and Miller, C. C. J. (2012). VAPB interacts with the mitochondrial protein PTPIP51 to regulate calcium homeostasis. *Hum. Mol. Genet.* **21**, 1299–311.

Dong, R., Saheki, Y., Swarup, S., Lucast, L., Harper, J. W. and De Camilli, P. (2016). Endosome-ER Contacts Control Actin Nucleation and Retromer Function through VAP-Dependent Regulation of PI4P. *Cell* **166**, 408–23.

Farkas, Á., De Laurentiis, E. I. and Schwappach, B. (2019). The natural history of Get3-like chaperones. *Traffic* **20**, 311–324.

Favaloro, V., Spasic, M., Schwappach, B. and Dobberstein, B. (2008). Distinct targeting pathways for the membrane insertion of tail-anchored (TA) proteins. *J. Cell Sci.* **121**, 1832–40.

Favaloro, V., Vilardi, F., Schlecht, R., Mayer, M. P. and Dobberstein, B. (2010). Asna1/TRC40-mediated membrane insertion of tail-anchored proteins. *J. Cell Sci.* **123**, 1522–30.

Figueiredo Costa, B., Cassella, P., Colombo, S. F. and Borgese, N. (2018). Discrimination between the endoplasmic reticulum and mitochondria by spontaneously inserting tail-anchored proteins. *Traffic* **19**, 182–197.

Flynn, J. M., Neher, S. B., Kim, Y. I., Sauer, R. T. and Baker, T. A. (2003). Proteomic discovery of cellular substrates of the ClpXP protease reveals five classes of ClpX-recognition signals. *Mol. Cell* **11**, 671–83.

Geiger, T., Wehner, A., Schaab, C., Cox, J. and Mann, M. (2012). Comparative Proteomic Analysis of Eleven Common Cell Lines Reveals Ubiquitous but Varying Expression of Most Proteins. *Mol. Cell. Proteomics* **11**, M111.014050.

Giaever, G., Chu, A. M., Ni, L., Connelly, C., Riles, L., Véronneau, S., Dow, S., Lucau-Danila, A., Anderson, K., André, B., et al. (2002). Functional profiling of the Saccharomyces cerevisiae genome. *Nature* **418**, 387–91.

Gillingham, A. K. and Munro, S. (2016). Finding the Golgi: Golgin Coiled-Coil Proteins Show the Way. *Trends Cell Biol.* **26**, 399–408.

Gristick, H. B., Rao, M., Chartron, J. W., Rome, M. E., Shan, S.-O. and Clemons, W. M. (2014). Crystal structure of ATP-bound Get3-Get4-Get5 complex reveals regulation of Get3 by Get4. *Nat. Struct. Mol. Biol.* **21**, 437–42.

Guna, A. and Hegde, R. S. (2018). Transmembrane Domain Recognition during Membrane Protein Biogenesis and Quality Control. *Curr. Biol.* **28**, R498–R511.

Guna, A., Volkmar, N., Christianson, J. C. and Hegde, R. S. (2018). The ER membrane protein complex is a transmembrane domain insertase. *Science* **359**, 470–473.

Haßdenteufel, S., Sicking, M., Schorr, S., Aviram, N., Fecher-Trost, C., Schuldiner, M., Jung, M., Zimmermann, R. and Lang, S. (2017). hSnd2 protein represents an alternative targeting factor to the endoplasmic reticulum in human cells. *FEBS Lett.* **591**, 3211–3224.

Hay, J. C., Chao, D. S., Kuo, C. S. and Scheller, R. H. (1997). Protein interactions regulating vesicle transport between the endoplasmic reticulum and Golgi apparatus in mammalian cells. *Cell* **89**, 149–58.

Honsho, M., Mitoma, J. Y. and Ito, A. (1998). Retention of cytochrome b5 in the endoplasmic reticulum is transmembrane and luminal domain-dependent. *J. Biol. Chem.* **273**, 20860–6.

Hu, J., Li, J., Qian, X., Denic, V. and Sha, B. (2009). The crystal structures of yeast Get3 suggest a mechanism for tail-anchored protein membrane insertion. *PLoS One* **4**, e8061.

Hua, R., Cheng, D., Coyaud, É., Freeman, S., Di Pietro, E., Wang, Y., Vissa, A., Yip, C. M., Fairn, G. D., Braverman, N., et al. (2017). VAPs and ACBD5 tether peroxisomes to the ER for peroxisome maintenance and lipid homeostasis. *J. Cell Biol.* **216**, 367–377.

Hui, N., Nakamura, N., Sönnichsen, B., Shima, D. T., Nilsson, T. and Warren, G. (1997). An isoform of the Golgi t-SNARE, syntaxin 5, with an endoplasmic reticulum retrieval signal. *Mol. Biol. Cell* **8**, 1777–87.

Jäntti, J., Keränen, S., Toikkanen, J., Kuismanen, E., Ehnholm, C., Söderlund, H. and Olkkonen, V. M. (1994). Membrane insertion and intracellular transport of yeast syntaxin Sso2p in mammalian cells. *J. Cell Sci.* **107 (Pt 1**, 3623–33.

Jessop, C. E., Watkins, R. H., Simmons, J. J., Tasab, M. and Bulleid, N. J. (2009). Protein disulphide isomerase family members show distinct substrate specificity: P5 is targeted to BiP client proteins. *J. Cell Sci.* **122**, 4287–95.

Johnson, N., Vilardi, F., Lang, S., Leznicki, P., Zimmermann, R. and High, S. (2012). TRC40 can deliver short secretory proteins to the Sec61 translocon. *J. Cell Sci.* **125**, 3612–20.

Johnson, N., Powis, K. and High, S. (2013). Post-translational translocation into the endoplasmic reticulum. *Biochim. Biophys. Acta - Mol. Cell Res.* **1833**, 2403–2409.

Jonikas, M. C., Collins, S. R., Denic, V., Oh, E., Quan, E. M., Schmid, V., Weibezahn, J., Schwappach, B., Walter, P., Weissman, J. S., et al. (2009). Comprehensive characterization of genes required for protein folding in the endoplasmic reticulum. *Science* **323**, 1693–1697.

Kalbfleisch, T., Cambon, A. and Wattenberg, B. W. (2007). A bioinformatics approach to identifying tail-anchored proteins in the human genome. *Traffic* **8**, 1687–1694.

Kasai, K., Suga, K., Izumi, T. and Akagawa, K. (2008). Syntaxin 8 has two functionally distinct di-leucine-based motifs. *Cell. Mol. Biol. Lett.* **13**, 144–54.

Kiktev, D. A., Patterson, J. C., Müller, S., Bariar, B., Pan, T. and Chernoff, Y. O. (2012). Regulation of chaperone effects on a yeast prion by cochaperone Sgt2. *Mol. Cell. Biol.* **32**, 4960–70.

Klebe, C., Bischoff, F. R., Ponstingl, H. and Wittinghofer, A. (1995). Interaction of the nuclear GTP-binding protein Ran with its regulatory proteins RCC1 and RanGAP1. *Biochemistry* **34**, 639–47.

Kline, C. F., Kurata, H. T., Hund, T. J., Cunha, S. R., Koval, O. M., Wright, P. J., Christensen, M., Anderson, M. E., Nichols, C. G. and Mohler, P. J. (2009). Dual role of K ATP channel C-terminal motif in membrane targeting and metabolic regulation. *Proc. Natl. Acad. Sci. U. S. A.* **106**, 16669–74.

Kubota, K., Yamagata, A., Sato, Y., Goto-Ito, S. and Fukai, S. (2012). Get1 stabilizes an open dimer conformation of get3 ATPase by binding two distinct interfaces. *J. Mol. Biol.* **422**, 366–75.

Kutay, U., Hartmann, E. and Rapoport, T. A. (1993). A class of membrane proteins with a C-terminal anchor. *Trends Cell Biol.* **3**, 72–5.

Kutay, U., Ahnert-Hilger, G., Hartmann, E., Wiedenmann, B. and Rapoport, T. A. (1995). Transport route for synaptobrevin via a novel pathway of insertion into the endoplasmic reticulum membrane. *EMBO J.* **14**, 217–23.

Kyte, J. and Doolittle, R. F. (1982). A simple method for displaying the hydropathic character of a protein. *J. Mol. Biol.* **157**, 105–32.

Lambert, J.-P., Ivosev, G., Couzens, A. L., Larsen, B., Taipale, M., Lin, Z.-Y., Zhong, Q., Lindquist, S., Vidal, M., Aebersold, R., et al. (2013). Mapping differential interactomes by affinity purification coupled with data-independent mass spectrometry acquisition. *Nat. Methods* **10**, 1239–45.

Lan, Y., Zhang, N., Liu, H., Xu, J. and Jiang, R. (2016). Golgb1 regulates protein glycosylation and is crucial for mammalian palate development. *Development* **143**, 2344–55.

Leznicki, P., Clancy, A., Schwappach, B. and High, S. (2010). Bat3 promotes the membrane integration of tail-anchored proteins. *J. Cell Sci.* **123**, 2170–2178.

Leznicki, P., Warwicker, J. and High, S. (2011). A biochemical analysis of the constraints of tail-anchored protein biogenesis. *Biochem. J.* **436**, 719–27.

Lin, S., Vollrath, M. A., Mangosing, S., Shen, J., Cardenas, E. and Corey, D. P. (2016). The zebrafish pinball wizard gene encodes WRB, a tail-anchored-protein receptor essential for inner-ear hair cells and retinal photoreceptors. *J. Physiol.* **594**, 895–914.

Linstedt, A. D., Foguet, M., Renz, M., Seelig, H. P., Glick, B. S. and Hauri, H. P. (1995). A C-terminally-anchored Golgi protein is inserted into the endoplasmic reticulum and then transported to the Golgi apparatus. *Proc. Natl. Acad. Sci. U. S. A.* **92**, 5102–5.

Manford, A. G., Stefan, C. J., Yuan, H. L., Macgurn, J. A. and Emr, S. D. (2012). ER-to-plasma membrane tethering proteins regulate cell signaling and ER morphology. *Dev. Cell* **23**, 1129–40.

Mariappan, M., Li, X., Stefanovic, S., Sharma, A., Mateja, A., Keenan, R. J. and Hegde, R. S. (2010). A ribosome-associating factor chaperones tail-anchored membrane proteins. *Nature* **466**, 1120–1124.

Mariappan, M., Mateja, A., Dobosz, M., Bove, E., Hegde, R. S. and Keenan, R. J. (2011). The mechanism of membrane-associated steps in tail-anchored protein insertion. *Nature* **477**, 61–6.

Masaki, R., Yamamoto, A. and Tashiro, Y. (1996). Membrane topology and retention of microsomal aldehyde dehydrogenase in the endoplasmic reticulum. *J. Biol. Chem.* **271**, 16939–44.

Mateja, A., Szlachcic, A., Downing, M. E., Dobosz, M., Mariappan, M., Hegde, R. S. and Keenan, R. J. (2009). The structural basis of tail-anchored membrane protein recognition by Get3. *Nature* **461**, 361–6.

Mateja, A., Paduch, M., Chang, H.-Y., Szydlowska, A., Kossiakoff, A. a., Hegde, R. S. and Keenan, R. J. (2015). Protein targeting. Structure of the Get3 targeting factor in complex with its membrane protein cargo. *Science* **347**, 1152–5.

McCune, B. T., Tang, W., Lu, J., Eaglesham, J. B., Thorne, L., Mayer, A. E., Condiff, E., Nice, T. J., Goodfellow, I., Krezel, A. M., et al. (2017). Noroviruses Co-opt the Function of Host Proteins VAPA and VAPB for Replication via a Phenylalanine-Phenylalanine-Acidic-Tract-Motif Mimic in Nonstructural Viral Protein NS1/2. *MBio* **8**, 1–17.

McGee, L. J., Jiang, A. L. and Lan, Y. (2017). Golga5 is dispensable for mouse embryonic development and postnatal survival. *Genesis* **55**, 1–8.

Metz, J., Wächter, A., Schmidt, B., Bujnicki, J. M. and Schwappach, B. (2006). The yeast Arr4p ATPase binds the chloride transporter Gef1p when copper is available in the cytosol. *J. Biol. Chem.* **281**, 410–7.

Mukhopadhyay, R., Ho, Y.-S., Swiatek, P. J., Rosen, B. P. and Bhattacharjee, H. (2006). Targeted disruption of the mouse Asna1 gene results in embryonic lethality. *FEBS Lett.* **580**, 3889–94.

Munro, S. (2011). The golgin coiled-coil proteins of the Golgi apparatus. *Cold Spring Harb. Perspect. Biol.* **3**, 1–14.

Nguyen, D., Stutz, R., Schorr, S., Lang, S., Pfeffer, S., Freeze, H. H., Förster, F., Helms, V., Dudek, J. and Zimmermann, R. (2018). Proteomics reveals signal peptide features determining the client specificity in human TRAP-dependent ER protein import. *Nat. Commun.* **9**, 3765.

Norlin, S., Parekh, V. S., Naredi, P. and Edlund, H. (2016). Asna1/TRC40 Controls β-Cell Function and Endoplasmic Reticulum Homeostasis by Ensuring Retrograde Transport. *Diabetes* **65**, 110–9.

Norlin, S., Parekh, V. and Edlund, H. (2018). The ATPase activity of Asna1/TRC40 is required for pancreatic progenitor cell survival. *Development* **145**, dev.154468.

Pedrazzini, E., Villa, A. and Borgese, N. (1996). A mutant cytochrome b5 with a lengthened membrane anchor escapes from the endoplasmic reticulum and reaches the plasma membrane. *Proc. Natl. Acad. Sci. U. S. A.* **93**, 4207–12.

Pedrazzini, E., Villa, A., Longhi, R., Bulbarelli, A. and Borgese, N. (2000). Mechanism of residence of cytochrome b(5), a tail-anchored protein, in the endoplasmic reticulum. *J. Cell Biol.* **148**, 899–914.

Pfaff, J., Rivera-Monroy, J., Jamieson, C., Rajanala, K., Vilardi, F., Schwappach, B. and Kehlenbach, R. H. (2016). Emery-Dreifuss muscular dystrophy mutations impair TRC40-mediated targeting of emerin to the inner nuclear membrane. *J. Cell Sci.* **129**, 502–16.

Plutner, H., Davidson, H. W., Saraste, J. and Balch, W. E. (1992). Morphological analysis of protein transport from the ER to Golgi membranes in digitonin-permeabilized cells: role of the P58 containing compartment. *J. Cell Biol.* **119**, 1097–116.

Powis, K., Schrul, B., Tienson, H., Gostimskaya, I., Breker, M., High, S., Schuldiner, M., Jakob, U. and Schwappach, B. (2013). Get3 is a holdase chaperone and moves to deposition sites for aggregated proteins when membrane targeting is blocked. *J. Cell Sci.* **126**, 473–83.

Prekeris, R., Yang, B., Oorschot, V., Klumperman, J. and Scheller, R. H. (1999). Differential roles of syntaxin 7 and syntaxin 8 in endosomal trafficking. *Mol. Biol. Cell* **10**, 3891–908.

Rabu, C., Wipf, P., Brodsky, J. L. and High, S. (2008). A precursor-specific role for Hsp40/Hsc70 during tail-anchored protein integration at the endoplasmic reticulum. *J. Biol. Chem.* **283**, 27504–13.

Rabu, C., Schmid, V., Schwappach, B. and High, S. (2009). Biogenesis of tail-anchored proteins: the beginning for the end? *J. Cell Sci.* **122**, 3605–12.

Rivera-Monroy, J., Musiol, L., Unthan-Fechner, K., Farkas, Á., Clancy, A., Coy-Vergara, J., Weill, U., Gockel, S., Lin, S.-Y., Corey, D. P., et al. (2016). Mice lacking WRB reveal differential biogenesis requirements of tail-anchored proteins in vivo. *Sci. Rep.* **6**, 39464.

Rocha, N., Kuijl, C., van der Kant, R., Janssen, L., Houben, D., Janssen, H., Zwart, W. and Neefjes, J. (2009). Cholesterol sensor ORP1L contacts the ER protein VAP to control Rab7-RILP-p150 Glued and late endosome positioning. *J. Cell Biol.* **185**, 1209–25.

Saraste, M., Sibbald, P. R. and Wittinghofer, A. (1990). The P-loop--a common motif in ATP- and GTP-binding proteins. *Trends Biochem. Sci.* **15**, 430–4.

Schneider, C. A., Rasband, W. S. and Eliceiri, K. W. (2012). NIH Image to ImageJ: 25 years of image analysis. *Nat. Methods* **9**, 671–5.

Schuldiner, M., Collins, S. R., Thompson, N. J., Denic, V., Bhamidipati, A., Punna, T., Ihmels, J., Andrews, B., Boone, C., Greenblatt, J. F., et al. (2005). Exploration of the function and organization of the yeast early secretory pathway through an epistatic miniarray profile. *Cell* **123**, 507–519.

Schuldiner, M., Metz, J., Schmid, V., Denic, V., Rakwalska, M., Schmitt, H. D., Schwappach, B. and Weissman, J. S. (2008). The GET complex mediates insertion of tail-anchored proteins into the ER membrane. *Cell* **134**, 634–45.

Shao, S., Rodrigo-Brenni, M. C., Kivlen, M. H. and Hegde, R. S. (2017). Mechanistic basis for a molecular triage reaction. *Science* **355**, 298–302.

Shen, J., Hsu, C.-M., Kang, B.-K., Rosen, B. P. and Bhattacharjee, H. (2003). The Saccharomyces cerevisiae Arr4p is involved in metal and heat tolerance. *Biometals* **16**, 369–78.

Shurtleff, M. J., Itzhak, D. N., Hussmann, J. A., Schirle Oakdale, N. T., Costa, E. A., Jonikas, M., Weibezahn, J., Popova, K. D., Jan, C. H., Sinitcyn, P., et al. (2018). The ER membrane protein complex interacts cotranslationally to enable biogenesis of multipass membrane proteins. *Elife* **7**,.

Simpson, P. J., Schwappach, B., Dohlman, H. G. and Isaacson, R. L. (2010). Structures of Get3, Get4, and Get5 provide new models for TA membrane protein targeting. *Structure* **18**, 897–902.

Stefanovic, S. and Hegde, R. S. (2007). Identification of a targeting factor for posttranslational membrane protein insertion into the ER. *Cell* **128**, 1147–59.

Stefer, S., Reitz, S., Wang, F., Wild, K., Pang, Y.-Y., Schwarz, D., Bomke, J., Hein, C., Löhr, F., Bernhard, F., et al. (2011). Structural basis for tail-anchored membrane protein biogenesis by the Get3-receptor complex. *Science* **333**, 758–62.

Stevenson, N. L., Bergen, D. J. M., Skinner, R. E. H., Kague, E., Martin-Silverstone, E., Robson Brown, K. A., Hammond, C. L. and Stephens, D. J. (2017). Giantin-knockout models reveal a feedback loop between Golgi function and glycosyltransferase expression. *J. Cell Sci.* **130**, 4132–4143.

Subramaniam, V. N., Loh, E., Horstmann, H., Habermann, A., Xu, Y., Coe, J., Griffiths, G. and Hong, W. (2000). Preferential association of syntaxin 8 with the early endosome. *J. Cell Sci.* **113 (Pt 6**, 997–1008.

Suloway, C. J. M., Chartron, J. W., Zaslaver, M. and Clemons, W. M. (2009). Model for eukaryotic tail-anchored protein binding based on the structure of Get3. *Proc. Natl. Acad. Sci. U. S. A.* **106**, 14849–54.

Tran, D. D., Russell, H. R., Sutor, S. L., van Deursen, J. and Bram, R. J. (2003). CAML is required for efficient EGF receptor recycling. *Dev. Cell* **5**, 245–56.

Vogl, C., Panou, I., Yamanbaeva, G., Wichmann, C., Mangosing, S. J., Vilardi, F., Indzhykulian, A. A., Pangršič, T., Santarelli, R., Rodriguez-Ballesteros, M., et al. (2016). Tryptophan-rich basic protein (WRB) mediates insertion of the tail-anchored protein otoferlin and is required for hair cell exocytosis and hearing. *EMBO J.* **35**, 2536–2552.

von Heijne, G. (2007). Formation of transmembrane helices in vivo--is hydrophobicity all that matters? *J. Gen. Physiol.* **129**, 353–6.

Voth, W., Schick, M., Gates, S., Li, S., Vilardi, F., Gostimskaya, I., Southworth, D. R., Schwappach, B. and Jakob, U. (2014). The protein targeting factor Get3 functions as ATP-independent chaperone under oxidative stress conditions. *Mol. Cell* **56**, 116–27.

Wang, F., Whynot, A., Tung, M. and Denic, V. (2011a). The Mechanism of Tail-Anchored Protein Insertion into the ER Membrane. *Mol. Cell* **43**, 738–750.

Wang, Q., Liu, Y., Soetandyo, N., Baek, K., Hegde, R. and Ye, Y. (2011b). A ubiquitin ligase-associated chaperone holdase maintains polypeptides in soluble states for proteasome degradation. *Mol. Cell* **42**, 758–70.

Wilson, R., Allen, A. J., Oliver, J., Brookman, J. L., High, S. and Bulleid, N. J. (1995). The translocation, folding, assembly and redox-dependent degradation of secretory and membrane proteins in semi-permeabilized mammalian cells. *Biochem. J.* **307 (Pt 3**, 679–87.

Yagita, Y., Hiromasa, T. and Fujiki, Y. (2013). Tail-anchored PEX26 targets peroxisomes via a PEX19-dependent and TRC40-independent class I pathway. *J. Cell Biol.* **200**, 651–66.

Yamagata, A., Mimura, H., Sato, Y., Yamashita, M., Yoshikawa, A. and Fukai, S. (2010). Structural insight into the membrane insertion of tail-anchored proteins by Get3. *Genes Cells* **15**, 29–41.

Yamamoto, Y. and Sakisaka, T. (2012). Molecular machinery for insertion of tail-anchored membrane proteins into the endoplasmic reticulum membrane in mammalian cells. *Mol. Cell* **48**, 387–97.

Zhang, Y., Bilbao, A., Bruderer, T., Luban, J., Strambio-De-Castillia, C., Lisacek, F., Hopfgartner, G. and Varesio, E. (2015). The Use of Variable Q1 Isolation Windows Improves Selectivity in LC-SWATH-MS Acquisition. *J. Proteome Res.* **14**, 4359–71.

Zhao, G. and London, E. (2006). An amino acid "transmembrane tendency" scale that approaches the theoretical limit to accuracy for prediction of transmembrane helices: relationship to biological hydrophobicity. *Protein Sci.* **15**, 1987–2001.

Zhou, T. and Rosen, B. P. (1999). Asp45 is a Mg2+ ligand in the ArsA ATPase. *J. Biol. Chem.* **274**, 13854–8.

Figures

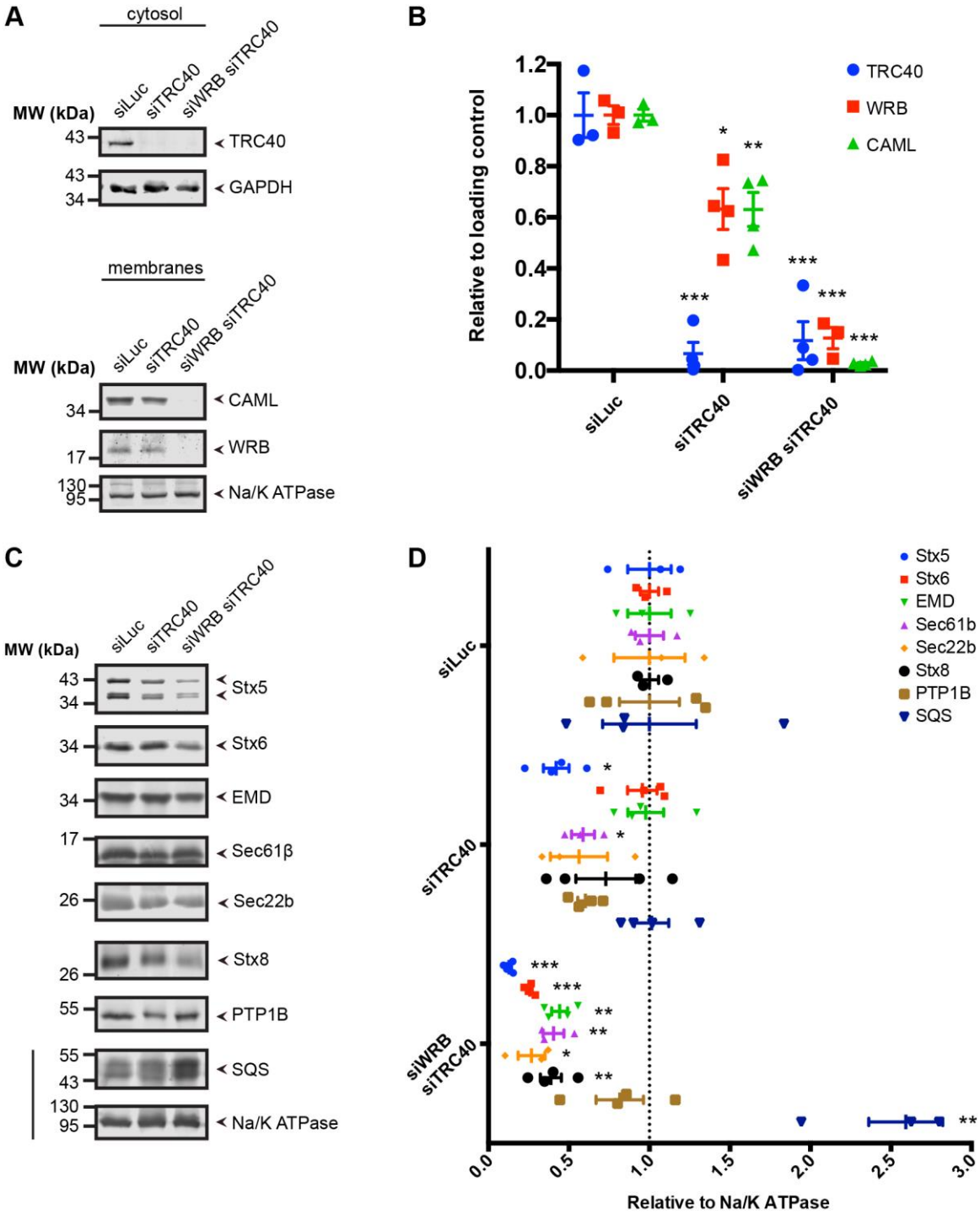

Figure 1

Silencing *WRB* and *TRC40* affects the steady-state levels of many TA-proteins. (A) Western blots demonstrating the down-regulation of *TRC40* and *WRB* upon transfection with previously characterized siRNAs (Pfaff et al., 2016; Rivera-Monroy et al., 2016; Yamamoto and Sakisaka, 2012). (B) Quantifications of Western blots shown in A ($n \geq 3$, mean and s.e.m. shown). (C) Western blots of the membrane fraction to detect steady-state levels of different TA-proteins after silencing *TRC40* or *TRC40* and *WRB*. The line indicates that the two panels are derived from the same lanes of the same gel. All other panels have a pertinent loading control used for the quantification but not shown here. (D) Quantifications of Western blots shown in C ($n \geq 3$, mean and s.e.m. shown). Statistics were determined by two-tailed *t*-test. Asterisks depict statistical significance (*$P<0.05$; **$P< 0.01$; ***$P<0.001$).

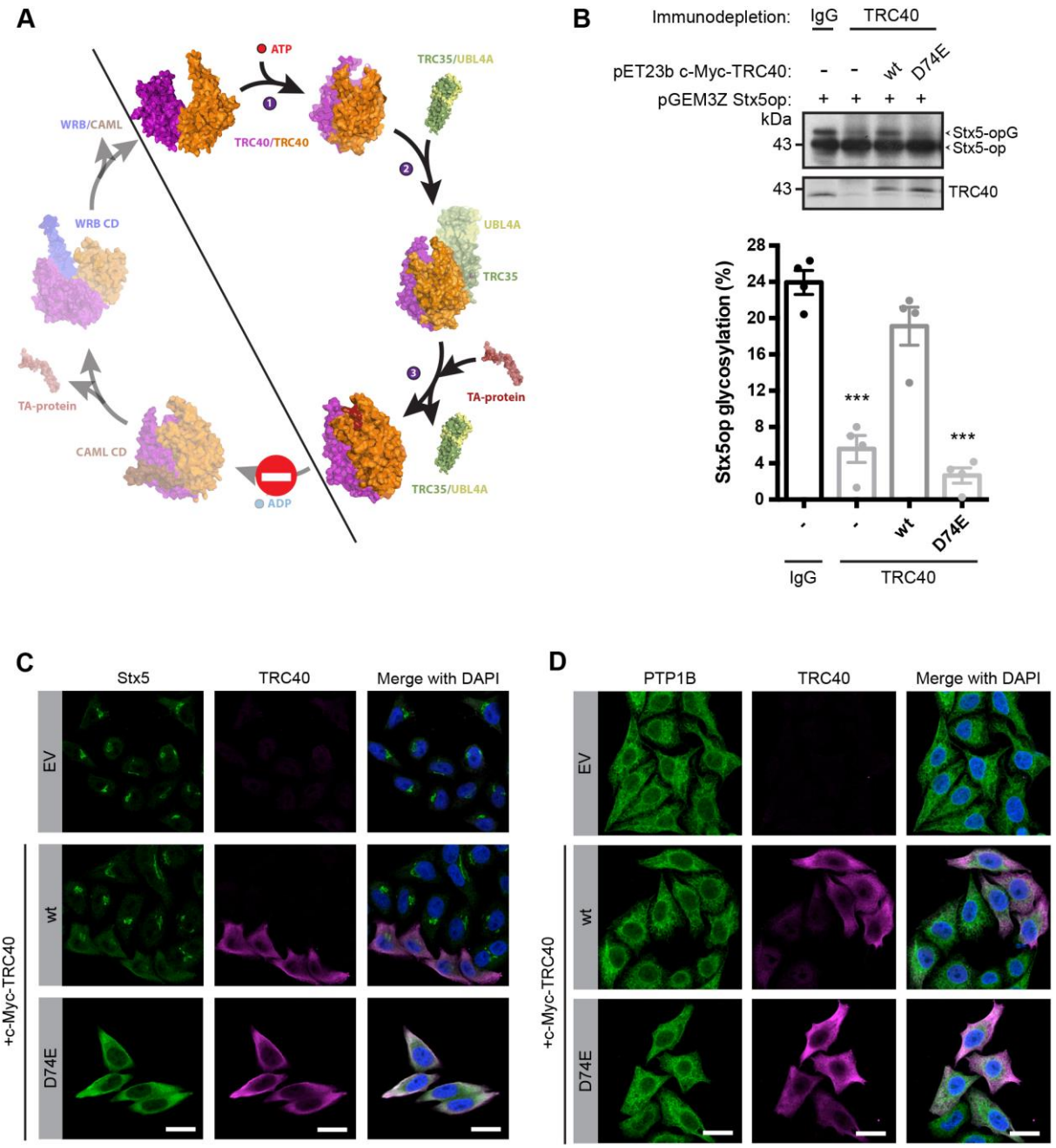

Figure 2

Over-expression of TRC40$_{D74E}$ leads to the mislocalization of Stx5. (A) Model of the TRC40 ATPase cycle based on structures representing different intermediates in the ATPase cycle of yeast Get3. The Protein Data Bank (PDB) IDs used for this scheme are the following: 3H84, 2WOJ, 4PWX, 2LPF, 4XTR, 3ZS9, 3SJB. (B) Stx5 insertion into canine microsomes was detected by the glycosylation of the C-terminal opsin tag. Opsin-tagged Stx5 was *in-vitro* translated in rabbit reticulocyte lysate, mock-depleted or TRC40-immunodepleted. In these lysates, c-Myc-TRC40 variants were first translated *in vitro* followed by the *in-vitro* translation

of opsin-tagged Stx5. Western blot was performed detecting the indicated proteins. Below: Quantification of Stx5 glycosylation, percentage of total (n=4, mean and s.e.m. shown). Statistics were determined by two-tailed t-test. Asterisks depict statistical significance (***P<0.001). (C,D) Immunofluorescence analysis of the subcellular localization of TA-proteins in HeLa cells over-expressing c-Myc-TRC40 variants. Transfection with the empty vector (EV) was used as negative control. Cells were fixed and stained for c-Myc-TRC40 (magenta, C,D), Stx5 (green, C), PTP1B (green, D) (n≥4). Scale bars: 20 μm.

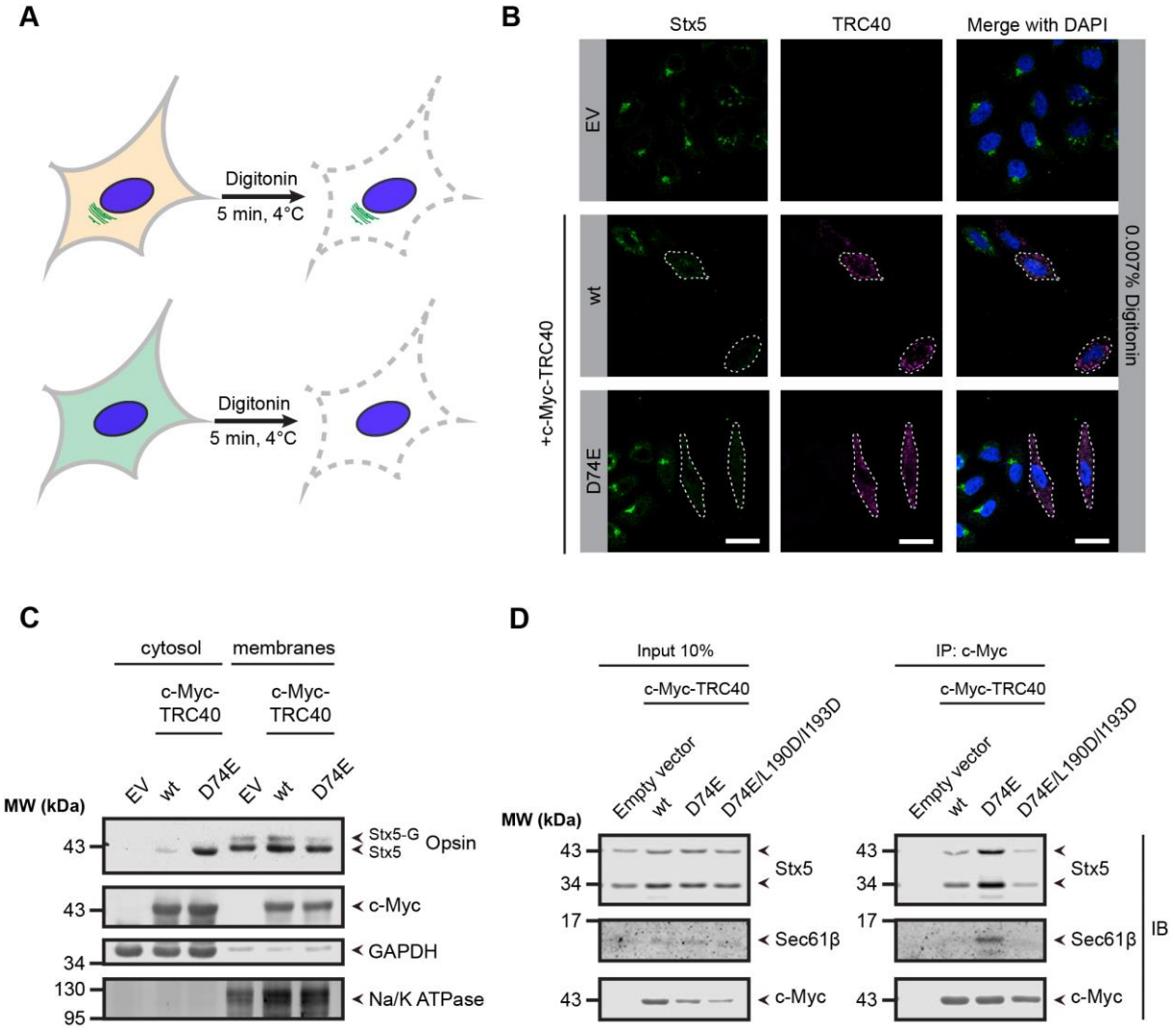

Figure 3

In the presence of TRC40$_{D74E}$ Stx5 accumulates in the cytoplasm. (A) Experimental strategy testing whether Stx5 was washed out in TRC40$_{D74E}$-transfected cells after treatment with digitonin. (B) Cells were semipermeabilized in the presence of a buffer containing 0.007% digitonin and then fixed. Cells were subjected to indirect immunofluorescence using antibodies against c-Myc (magenta) and Stx5 (green) (*n*=3). Dashed lines outline c-Myc-TRC40-transfected cells. Scale bars: 20 µm. (C) Stx5 accumulated in the cytosol of cells over-expressing TRC40$_{D74E}$. Cell lysates from the Stx5-opsin stable cell line were subjected to fractionation. Cells were transfected with either c-Myc-TRC40 or c-Myc-TRC40$_{D74E}$. Transfection with the empty vector (EV) was used as negative control. Subsequently, the expression of Stx5-opsin was induced with 1 µg/mL of tetracycline (Tet) for 6 h. Western blot was performed detecting the indicated proteins (*n*=3). (D) Co-immunoprecipitation from

cytosol in the absence of detergent shows that TRC40$_{D74E}$ interacts with TA-proteins such as Stx5 and Sec61β. Cells were transfected with c-Myc-TRC40 variants using the empty vector (EV) as negative control. Western blot was performed detecting the indicated proteins. Note that endogenous Stx5 migrates as two different bands due to alternative start codons (Hui et al., 1997) (*n*=3).

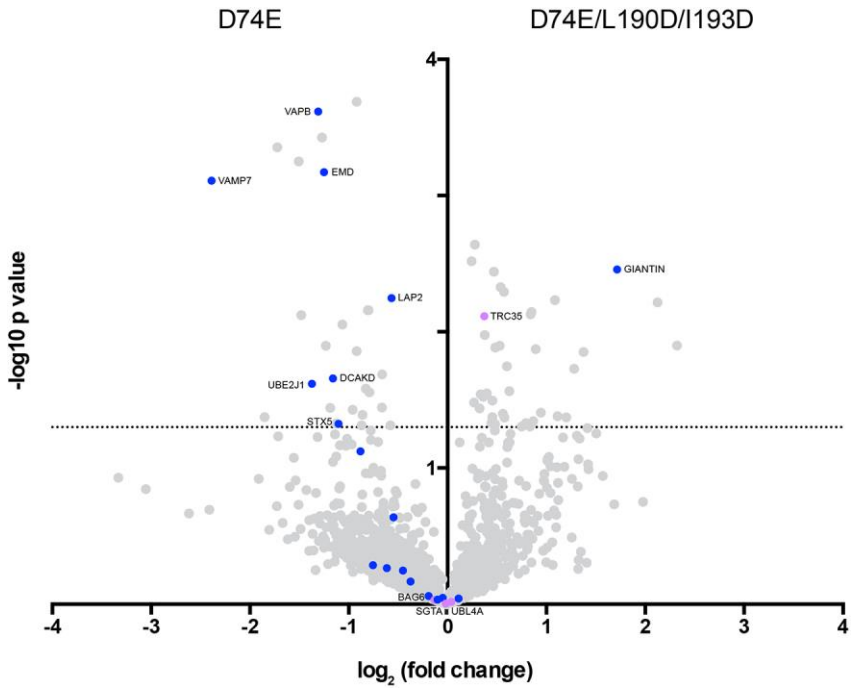

Figure 4

Unbiased SWATH mass spectrometry analysis reveals additional TA-substrates. $TRC40_{D74E}$ TA-protein enrichment compared to the mutant manipulating the TA-binding groove, $TRC40_{D74E/L190D/I193D}$. Volcano-plot for c-Myc-TRC40 SWATH-based interactome (n=3). TRC pathway components are labelled in magenta, TA-proteins in blue. The dotted line indicates statistical significance (P<0.05). Statistics were determined by two-tailed t-test.

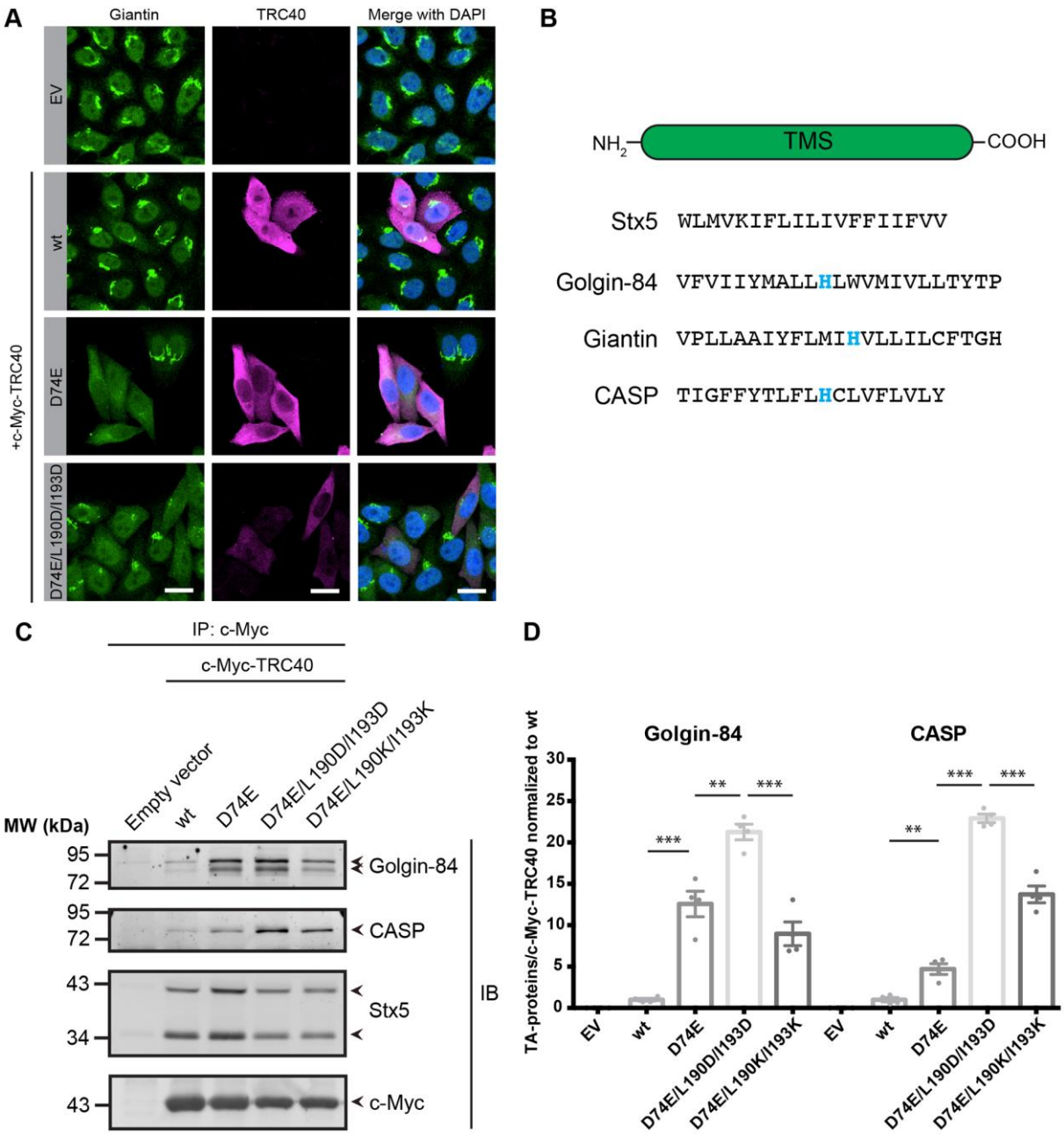

Figure 5

TA-golgins are trapped by TRC40$_{D74E}$. (A) HeLa cells were transfected to express c-Myc-TRC40 constructs and later processed for indirect immunofluorescence using antibodies against c-Myc (magenta) and giantin (green) (*n*=3). Transfection with the empty vector (EV) was used as negative control. Scale bars: 20 µm. (B) Comparison of TMS of the TA-golgins. (C) Co-immunoprecipitation from cytosol in the absence of detergent shows that TRC40$_{D74E}$ interacts with TA-proteins such as golgin-84 and CASP. Cells were transfected with c-Myc-TRC40

variants using the empty vector (EV) as negative control. Western blot was performed detecting the indicated proteins. (D) Quantifications of Western blots shown in C (n=4, mean and s.e.m. shown). Statistics were determined by two-tailed t-test. Asterisks indicate statistical significance (**P< 0.01; ***P<0.001).

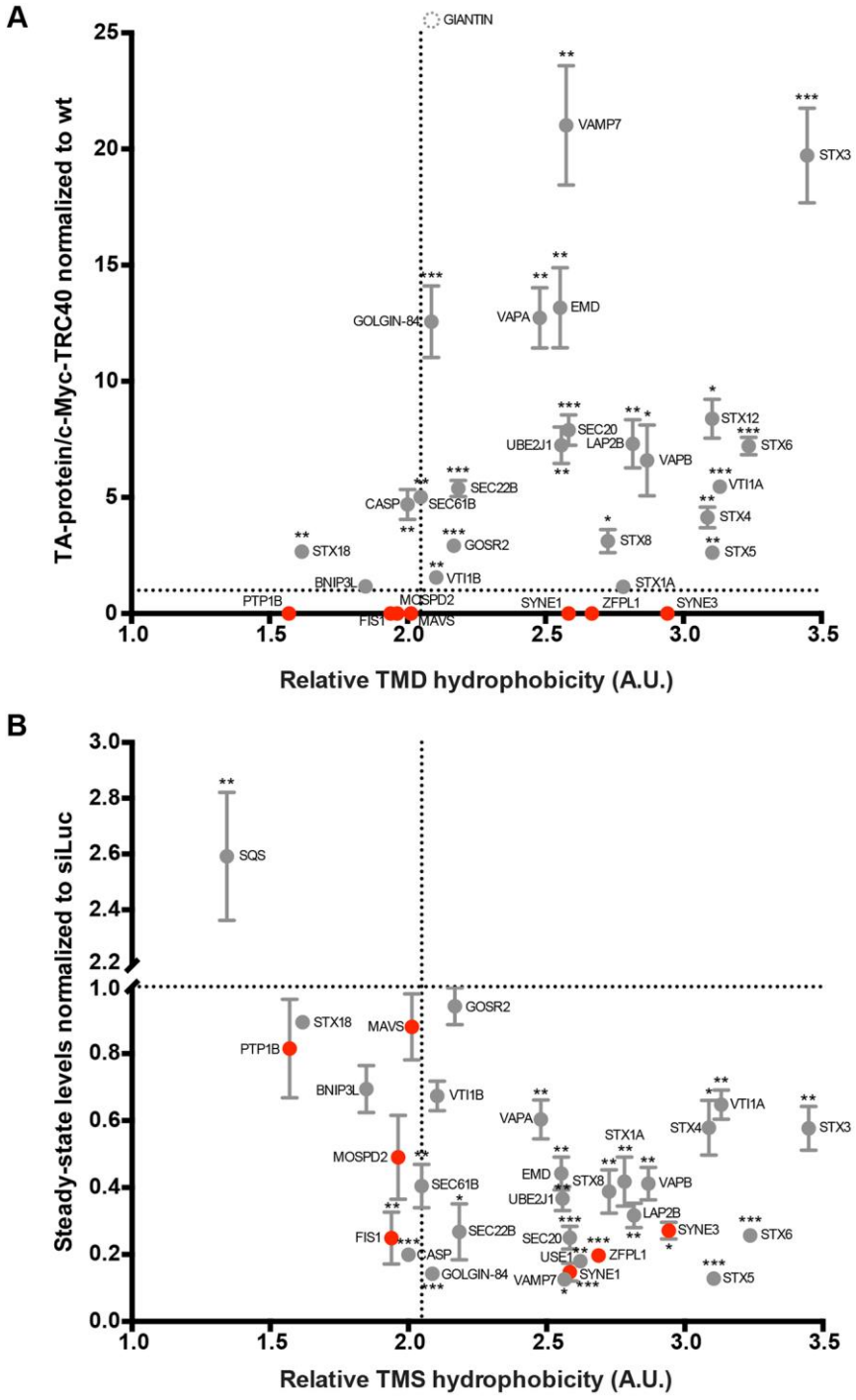

Figure 6

TMS hydrophobicity determines but does not fully explain TRC40-dependence. (A) Summary of the trapping efficiency observed for different TA-proteins with c-Myc-TRC40$_{D74E}$ as compared to wild type c-Myc-TRC40 ($n \geq 3$, mean and s.e.m. shown) plotted against the hydrophobicity score of the TMS (GRAVY) (Kyte and Doolittle, 1982). (B) Effects of combined siRNA-mediated down-regulation of *TRC40* and *WRB* on the depicted TA-proteins ($n \geq 3$, mean and s.e.m. shown) according to their relative TMS hydrophobicity score according

to the GRAVY scale. Statistics were determined by two-tailed *t*-test. Asterisks depict statistical significance (*P<0.05; **P<0.01; ***P<0.001). Giantin is depicted with a dashed symbol on top of the scheme to indicate its TMS hydrophobicity score similar to the other two TA-golgins. The dotted line (x axes) indicates the hydrophobicity score of Sec61β TMS and (y axes) the same ratio of TA-protein normalized to the pertinent control. TA-proteins that were not trapped by TRC40$_{D74E}$ are depicted in red.

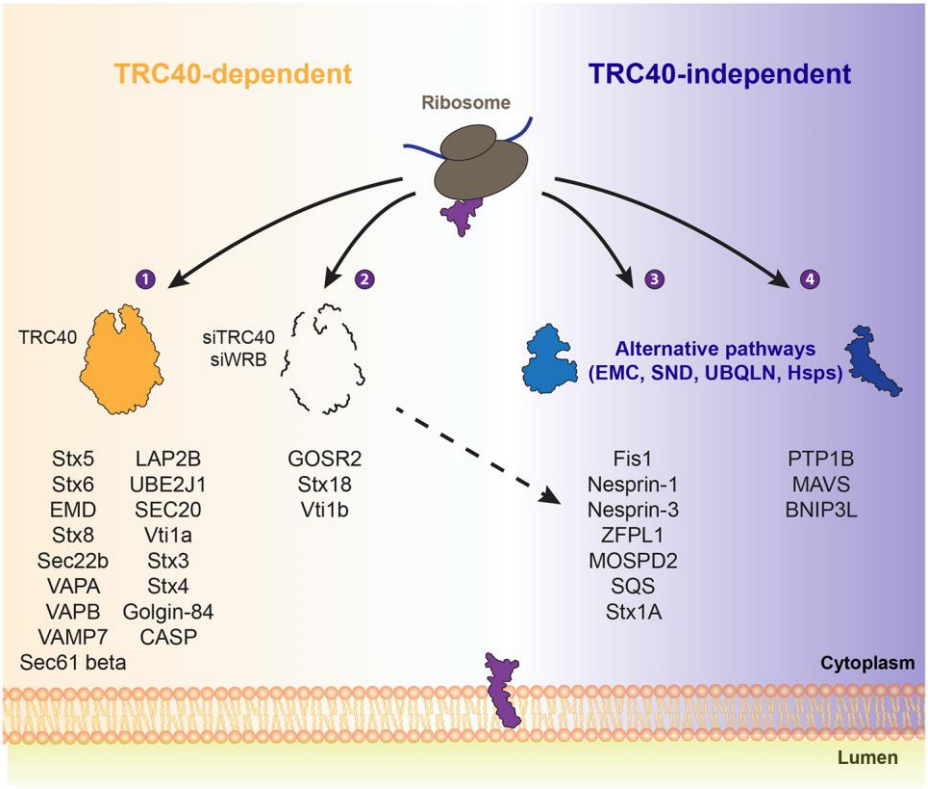

Figure 7

TRC40-dependence of TA-protein targeting. Based on the interaction with TRC40$_{D74E}$ and the steady-state levels when the TRC pathway is impaired (Figs 1,4,5,6,S2,S3,S4,S6,S7), TA-proteins can be categorized in the following groups: (1) Substrates can interact with TRC40$_{D74E}$ and they are affected at the steady-state when the pathway is downregulated. Therefore, TRC40 is likely involved in the targeting of those proteins. (2) These TA-proteins can interact with TRC40$_{D74E}$ but they remain unaltered upon the knockdown of the pathway. Even though they can interact with TRC40, there is redundancy and robust targeting in the absence of the TRC pathway. (3) Despite of the lack of interaction with TRC40, the combined knockdown of *WRB* and *TRC40* affects the steady-state levels of this group of TA-proteins. Hence, the decrease of their protein steady-state levels most likely reflects an indirect effect. (4) Other pathways target these TA-proteins that are unable to interact with TRC40 and their steady-state levels are unaffected when the TRC pathway is impaired.

Table 1

Identification of selected TA-proteins in TRC40$_{D74E}$ immunoprecipitates. The presence of candidate TA-proteins was assessed by Western blotting based on the availability of antibodies (compare Table S1). The TMS hydrophobicity score was calculated according to the GRAVY scale. Statistical significance was determined by two-tailed *t*-test.

Gene symbol	Protein name	TMS hydrophobicity	Fold change	p-value
VTI1A	Vesicle transport through interaction with t-SNAREs homolog 1A	3.132	5.464	6.7295E-06
STX6	Syntaxin-6	3.237	7.211	8.5147E-05
GOSR2	Golgi SNAP receptor complex member 2	2.168	2.918	2.70E-04
SEC22B	Vesicle-trafficking protein SEC22b	2.184	5.382	4.71E-04
SEC20	Vesicle transport protein SEC20 isoform BNIP1	2.584	7.899	4.76E-04
GOLGIN-84	Golgin subfamily A member 5	2.087	12.568	3.03E-04
STX3	Syntaxin-3	3.448	19.717	1.21E-04
SEC61B	Protein transport protein Sec61 subunit beta	2.048	5.016	1.21E-03
STX18	Syntaxin-18	1.617	2.672	1.25E-03
VAMP7	Vesicle-associated membrane protein 7 isoform 1	2.575	21.021	1.63E-03
CASP	Protein CASP	2.000	4.699	1.80E-03
STX5	Syntaxin-5	3.105	2.625	0.002
VAPA	Vesicle-associated membrane protein-associated protein A	2.479	12.732	0.002
EMD	Emerin	2.553	13.165	0.002
UBE2J1	Ubiquitin-conjugating enzyme E2, J1	2.558	7.246	0.002
LAP2B	Lamina-associated polypeptide 2, isoform beta	2.816	7.304	0.004
STX4	Syntaxin-4	3.087	4.136	0.006
VTI1B	Vesicle transport through interaction with t-SNAREs 1B	2.104	1.551	0.006
STX12	Syntaxin-12	3.104	8.390	0.013
STX8	Syntaxin-8	2.726	3.125	0.013
VAPB	Vesicle-associated membrane protein-associated protein B/C	2.868	6.590	0.028
STX1A	Syntaxin-1A	2.782	1.149	0.154
BNIP3L	BCL2/adenovirus E1B 19kD-interacting protein 3-like	1.848	1.175	0.252

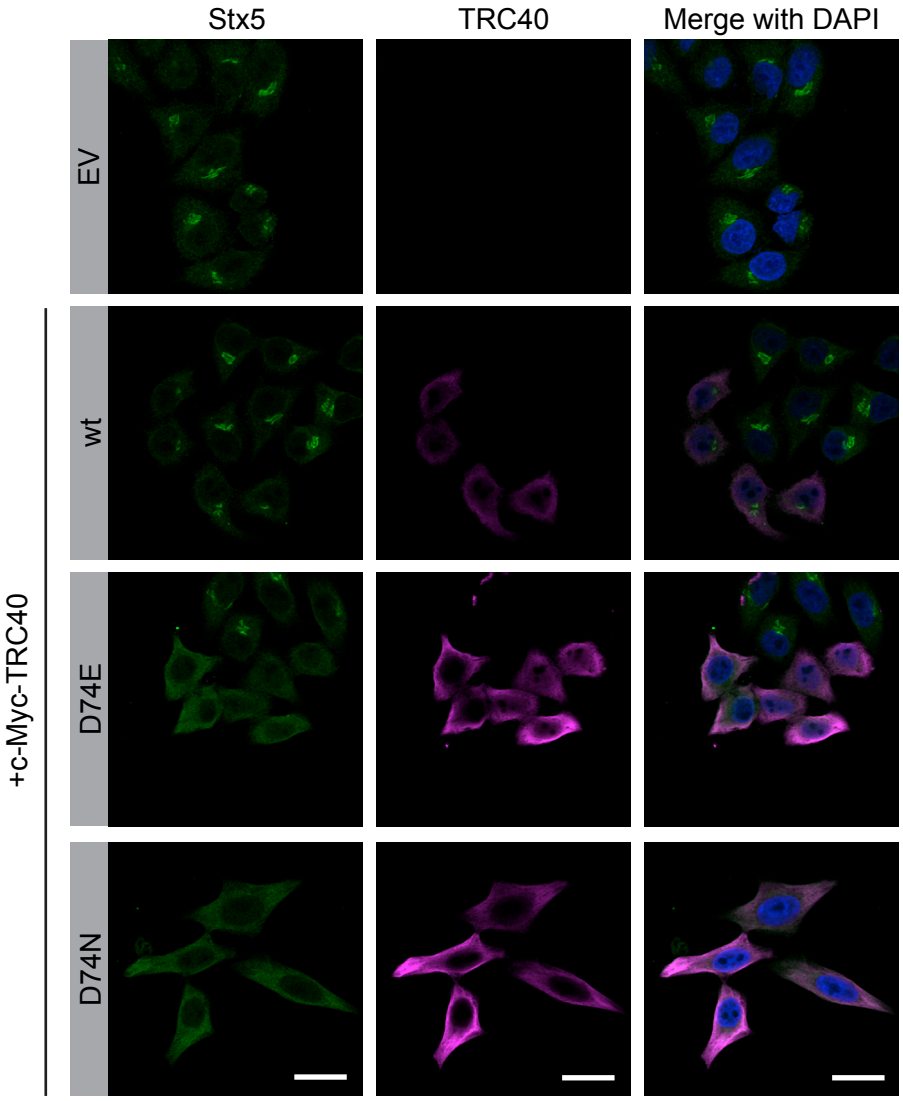

Figure S1. In the presence of TRC40$_{D74N}$ Stx5 accumulates in cytoplasm.
HeLa cells were transfected to express c-Myc-TRC40 constructs and later processed for indirect immunofluorescence using antibodies against TRC40 (magenta) and Stx5 (green). Transfection with the empty vector (EV) was used as negative control. The signal observed from endogenous TRC40 was close to background and it is therefore not visible with the settings used. Three independent biological replicates were analyzed. Scale bars: 20 µm.

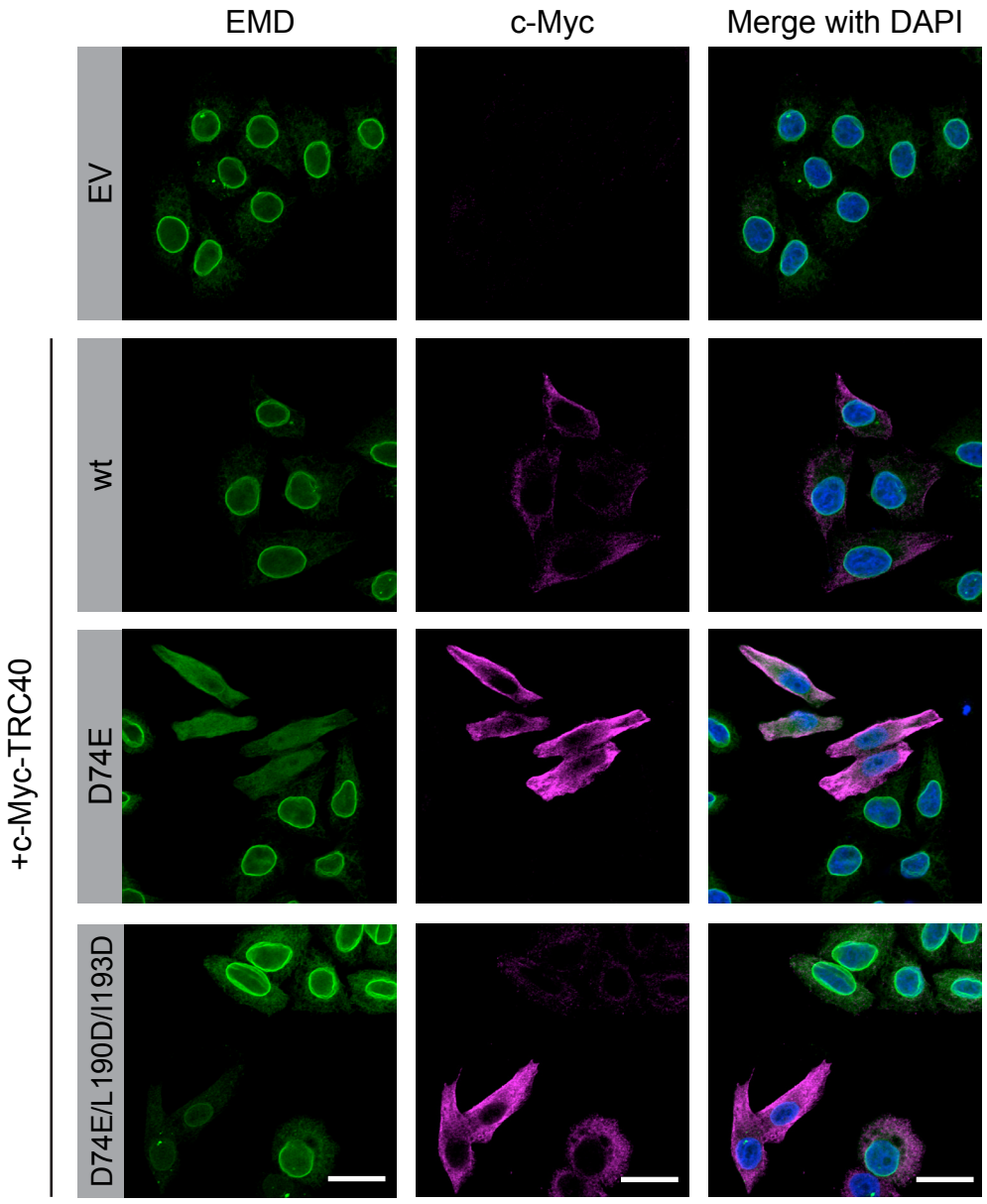

Figure S2. TRC40$_{D74E}$ traps EMD in the cytoplasm.
HeLa cells were transfected to express c-Myc-TRC40 constructs. Cells were subjected to indirect immunofluorescence using antibodies against c-Myc (magenta) and Stx5 (green). Three independent biological replicates were analyzed. Scale bars: 20 µm.

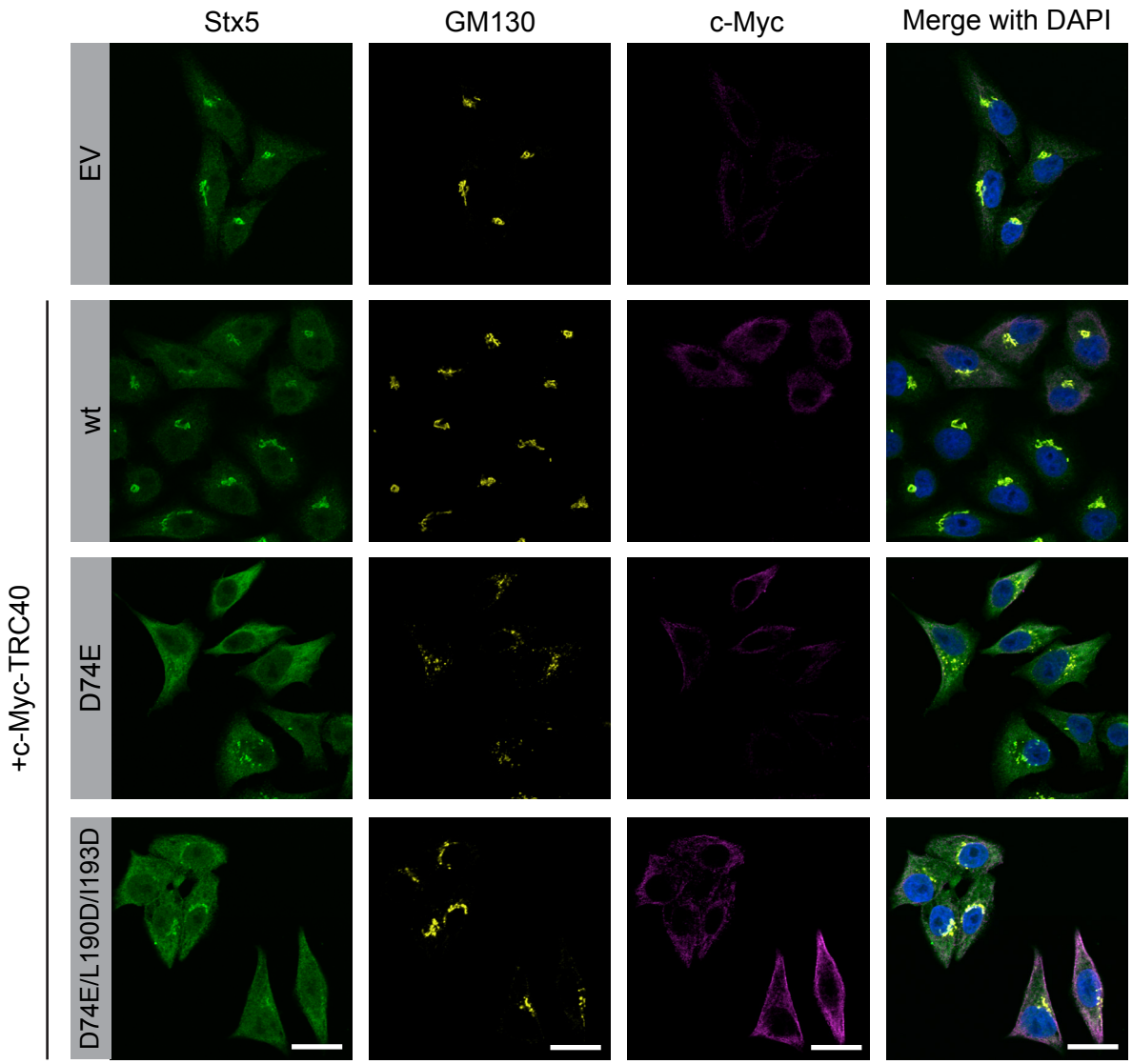

Figure S3. A double mutation in the TA-binding groove of TRC40$_{D74E}$ partially restores Stx5 localization.
HeLa cells were transfected to express c-Myc-TRC40 constructs. Cells were subjected to indirect immunofluorescence using antibodies against c-Myc (magenta), the *cis*-Golgi marker GM130 (yellow) and Stx5 (green). Three independent biological replicates were analyzed. Scale bars: 20 µm.

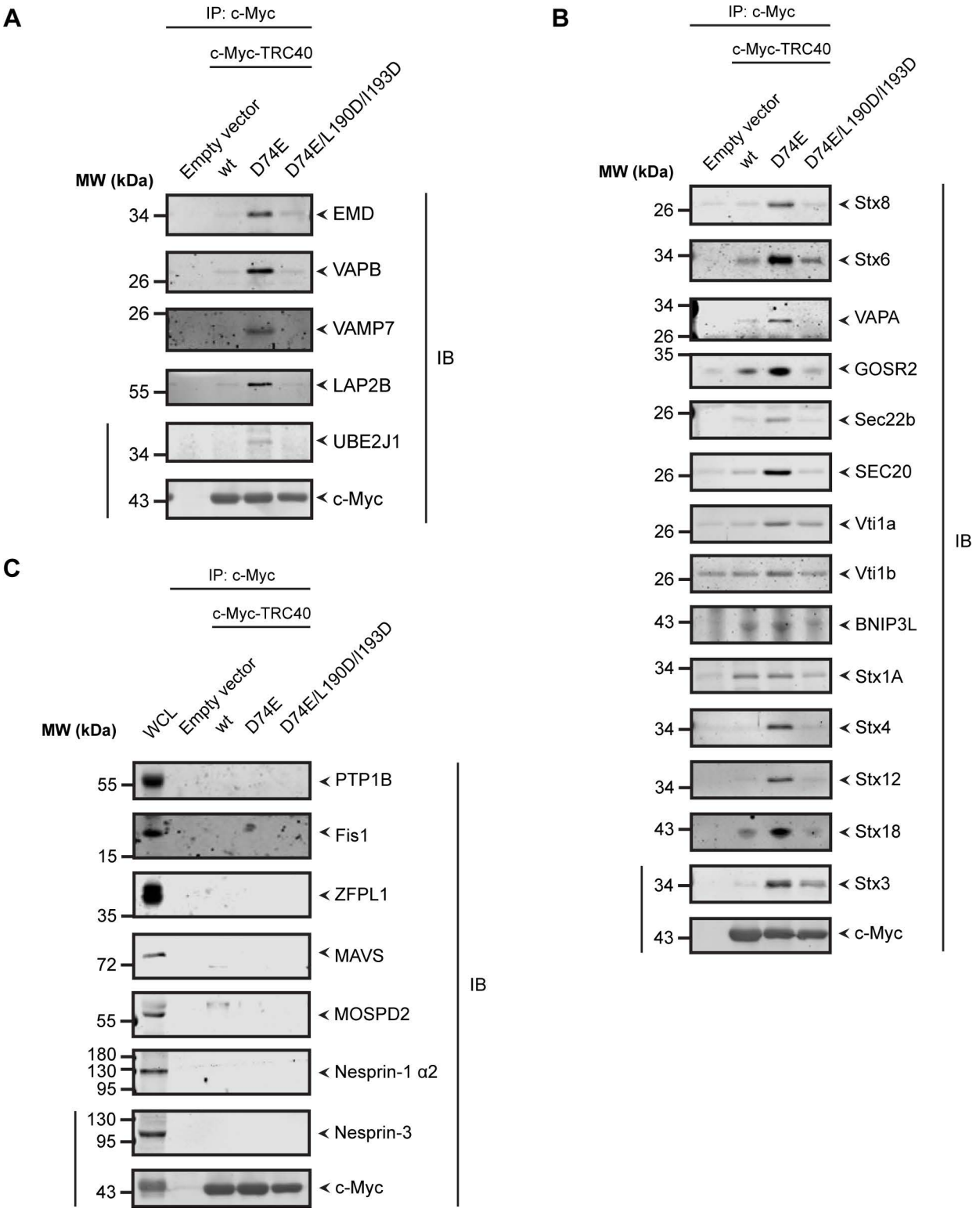

Figure S4. Candidate testing reveals many TA proteins interacting with the TRC40 trap mutant via the TA-binding groove.

(A-B) Co-immunoprecipitation from cytosol in the absence of detergent shows that $TRC40_{D74E}$ interacts with many TA-proteins. Cells were transfected with either c-Myc-TRC40, c-Myc-$TRC40_{D74E}$ or c-Myc-$TRC40_{D74E/L190D/I193D}$ using the empty vector (EV) as negative control. Western blot was performed detecting the indicated proteins. Three independent biological replicates were analyzed. The line indicates that the two panels are derived from the same lanes of the same gel. All other panels have a pertinent bait control used for the quantification but not shown here.(C) Detection of PTP1B, Fis1, ZFPL1, MAVS, MOSPD2, Nesprin-1 alpha 2 isoform and Nesprin-3 in the co-immunoprecipitated material reveals their absence from the c-Myc immuno-precipitates. Whole cell lysate (WCL) indicates the presence of the proteins in the transfected cells. The line indicates that the two panels are derived from the same lanes of the same gel. All other panels have a pertinent bait control used for the quantification but not shown here.

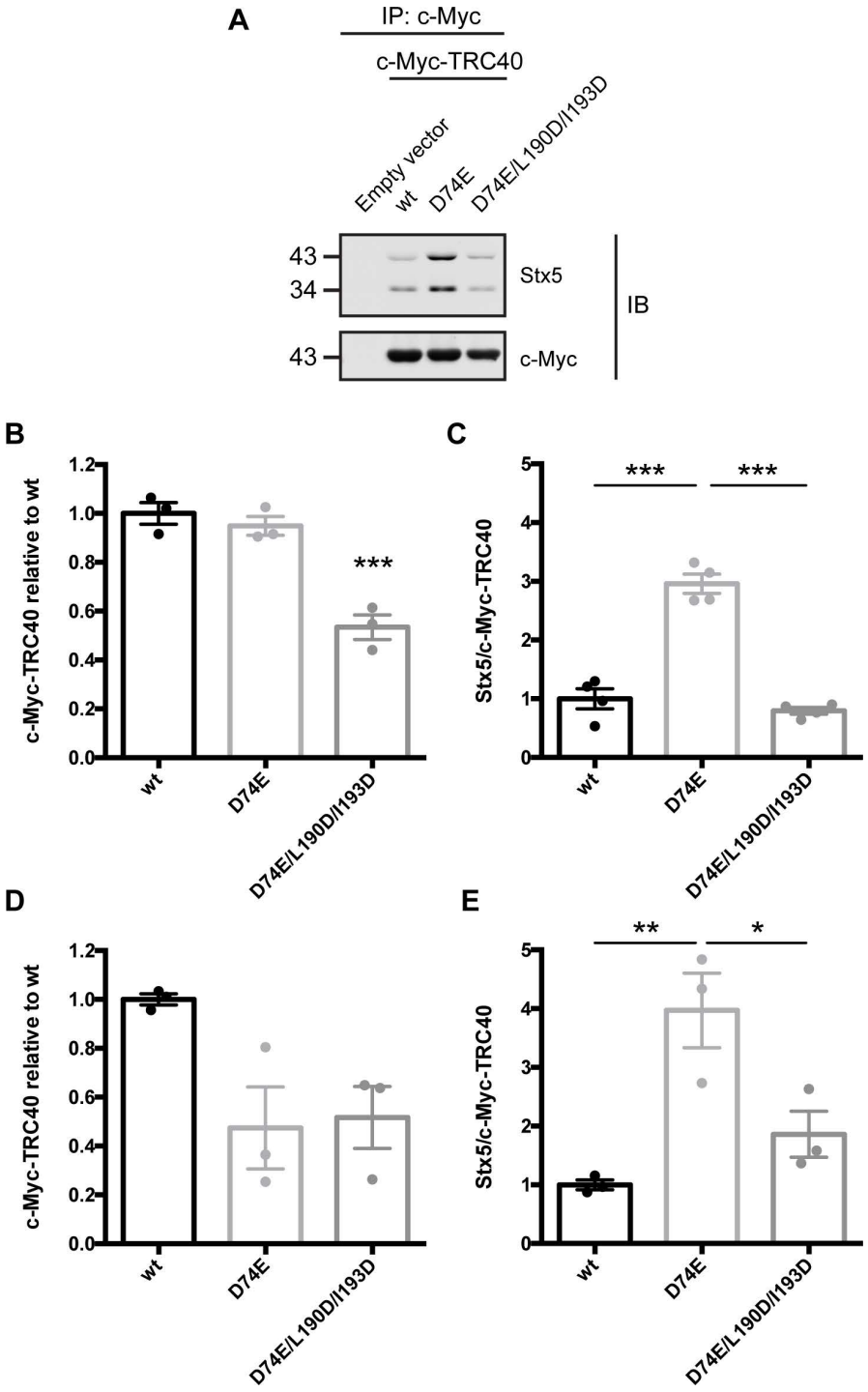

Figure S5. Quantitative SWATH mass spectrometry confirms TA-binding groove dependent enrichment of Stx5 with TRC40$_{D74E}$.
(A) Representative Western blots of eluates from anti-c-Myc-immunoprecipitation detecting the immunoprecipitated TRC40 variants and the co-precipitating TA protein Stx5. Note that endogenous Stx5 migrates as two different bands due to alternative start codons (Hui et al., 1997). At least three independent biological replicates were analyzed. (B) Quantification of c-Myc signal in immunoprecipitated material. The graph shows the mean and the error bars depict +-s.e.m.. Statistics were determined by two-tailed Student's *t*-test. Asterisks indicate statistical significance (*** $P < 0.001$). (C) Quantification of ratio between co-immunoprecipitated Stx5 and TRC40 variants. The graph shows the mean and the error bars depict +-s.e.m.. Statistics were determined by two-tailed Student's *t*-test. Asterisks indicate statistical significance (*** $P < 0.001$). (D) Peptide-based quantification of TRC40 variants from SWATH mass spectrometry analysis. Three independent biological replicates were analyzed. The graph shows the mean and the error bars depict +-s.e.m. (E) Quantification of ratio between co-immunoprecipitated Stx5 and TRC40 variants as obtained by SWATH mass spectrometry analysis. The graph shows the mean and the error bars depict +-s.e.m.. Statistics were determined by two-tailed Student's *t*-test. Asterisks indicate statistical significance (* $P < 0.05$; ** $P < 0.01$).

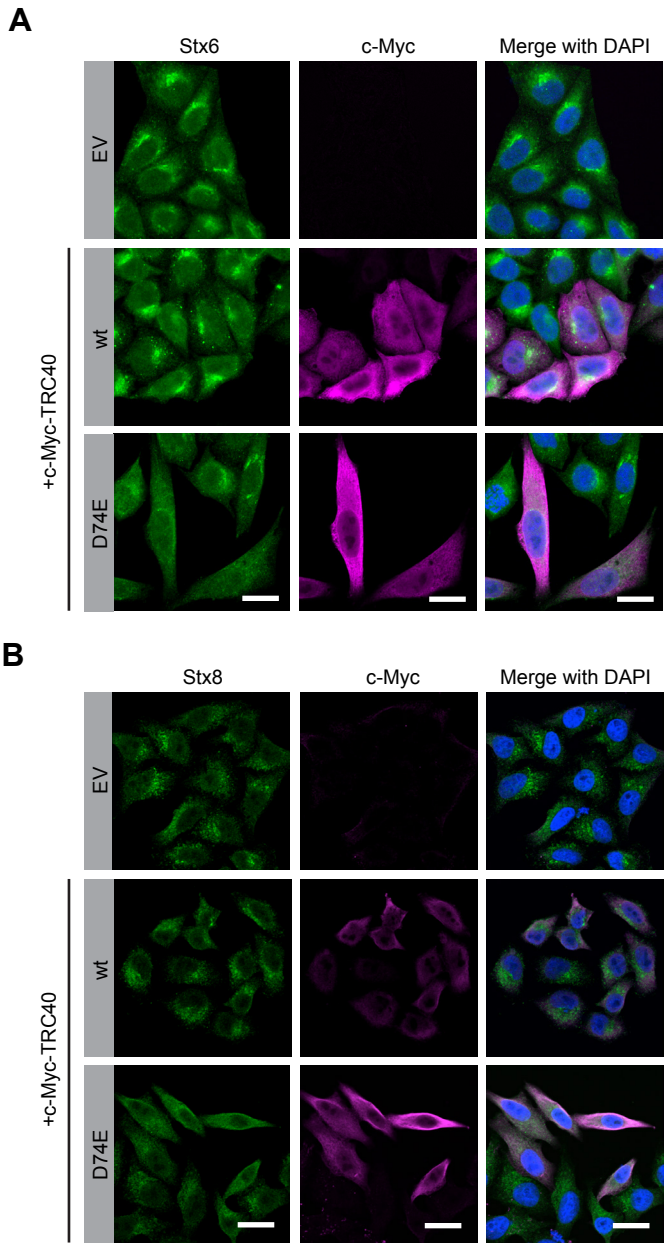

Figure S6. Stx6 and Stx8 are partially mislocalized upon over-expression of the TRC40 trap.

(A-B) HeLa cells were transfected to express c-Myc-TRC40 constructs and later processed for indirect immunofluorescence using antibodies against c-Myc (magenta), Stx6 (green, A) and Stx8 (green, B). Transfection with the empty vector (EV) was used as negative control. Three independent biological replicates were analyzed. Scale bars: 20 µm.

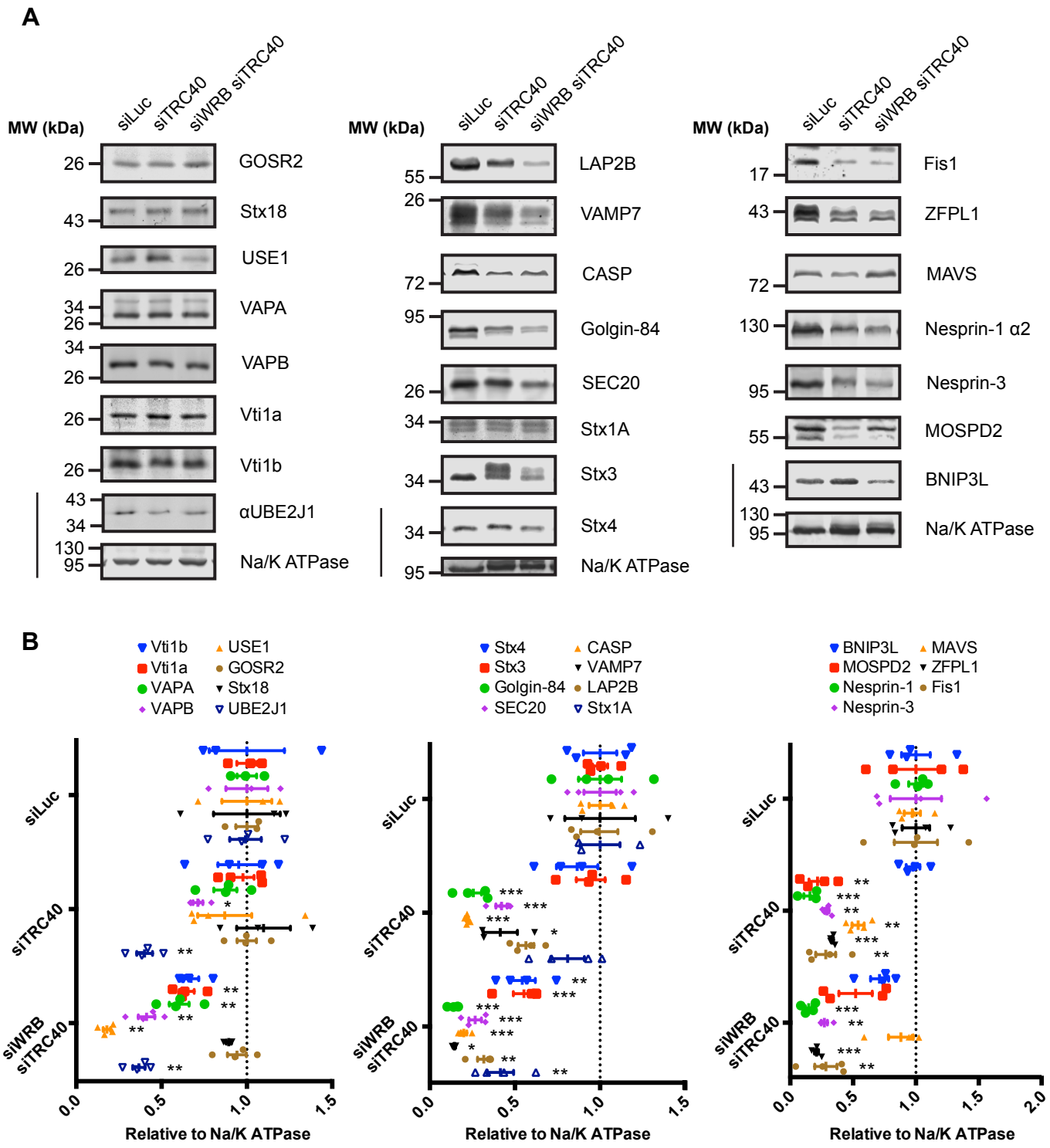

Figure S7. Silencing *WRB* and *TRC40* affects the steady-state levels of many TA proteins.

(A) Exemplary Western blots of the steady-state levels of different TA proteins after silencing *TRC40* or *TRC40* and *WRB*. The line indicates that the two panels are derived from the same lanes of the same gel. All other panels have a pertinent loading control used for the quantification but not shown here. (B) Quantifications of Western blots shown in A. All experiments were performed at least in biological triplicates. The plots depict the mean +- s.e.m.. Statistics were determined by two-tailed Student's *t*-test. Asterisks depict statistical significance (* $P <$ 0.05; ** $P <$ 0.01; *** $P <$ 0.001). The dotted line indicates the siLuc steady-state levels.

Table S1. List of primary and secondary antibodies used in this study.

Name	Raised in	Company	Catalog no.	Lot #	Dilution (WB)	Dilution (IF)
BNIP3L	mouse	Invitrogen	39-3300	QC215886	1:250	
CAML	guinea pig	Synaptic Systems	359 004	359004/1	1:1000	
CASP	rabbit	Proteintech	11733-1-AP	50220	1:1000	
Emerin	rabbit	Santa Cruz	sc-15378	H1115	1:1000	1:150
Fis1	rabbit	Thermo Fisher	PA1-41082	QC1999106	1:1000	
GAPDH	mouse	NeoBiotech	NB-29-00852	16/06-G4-C5	1:40000	
Giantin	guinea pig	Synaptic Systems	263005	263005/1		1:200
GM130	mouse	BD Transduction Laboratories	610823	24277		1:300
Golgin-84	rabbit	Sigma-Aldrich	HPA000992	A104695	1:1000	
GOSR2	rabbit	Synaptic Systems	170003	170003/4	1:1000	
Lamin-A/C	mouse	abcam	ab40567			1:200
LAP2B	rabbit	Sigma-Aldrich	SAB2102484	QC14874	1:1500	
MAVS	mouse	Santa Cruz	sc-166583	L0417	1:500	
MOSPD2	rabbit	abcam	ab129250	GR89338-4	1:500	
c-Myc	mouse	Santa Cruz	sc-40	B0116	1:1000	1:200
c-Myc	rabbit	Santa Cruz	sc-789	I171		1:200
Na+/K+-ATPase α1	mouse	Santa Cruz	sc-21712	B1516	1:1000	
Nesprin-1	rabbit	abcam	ab192234	GR181158-5	1:1000	
Nesprin-3	rabbit	abcam	ab186751	GR163090-1	1:1000	
Opsin	mouse	From Bernhard Dobberstein			1:1000	
PTP1B	rabbit	Sigma-Aldrich	HPA012542		1:1000	1:100
SEC20	rabbit	abcam	ab151551	YJ081322CS	1:1000	
Sec22b	rabbit	Synaptic Systems	186003	186003/1-8	1:1000	
Sec61β	rabbit	From Bernhard Dobberstein			1:1000	1:300
Squalene synthase	mouse	Santa Cruz	sc-271602	D2816	1:1000	
Syntaxin 1	mouse	Synaptic Systems	110011	110011/13	1:1000	
Syntaxin 3	rabbit	Synaptic Systems	110033	110033/24	1:750	
Syntaxin 4	rabbit	Synaptic Systems	110041	110041/2	1:1000	
Syntaxin 5	rabbit	Synaptic Systems	110053	110053/16	1:2000	1:250
Syntaxin 6	rabbit	Synaptic Systems	110062	110062/9	1:1000	1:300
Syntaxin 8	rabbit	Synaptic Systems	110083	110083/1-11	1:1000	1:300
Syntaxin 12	rabbit	Synaptic Systems	110133	110133/2	1:1000	

Syntaxin 18	rabbit	Synaptic Systems	110183	110183/3	1:1000	
TRC40	mouse	Sigma-Aldrich	WH0000439M3	D3011-2H3	1:1000	1:100
TRC40	rabbit	Proteintech	15450-1-AP	00021130	1:1000	
TRC40 #4	rabbit	From Bernhard Dobberstein			1:1000	
UBE2J1	mouse	Santa Cruz	sc-377002	H2917	1:1000	
USE1	rabbit	Proteintech	25218-1-AP	00022214	1:1000	
VAMP7	rabbit	Synaptic Systems	232003	232003/2-9	1:1000	
VAPA	rabbit	Proteintech	15275-1-AP	00022782	1:1000	
VAPB	rabbit	Proteintech	14477-1-AP	00013727	1:1000	
Vti1a	rabbit	Synaptic Systems	165003	165003/1	1:1000	
Vti1b	rabbit	Synaptic Systems	164002	164002/7	1:1000	
WRB	rabbit	Synaptic Systems	324002	324002/1-2	1:500	
ZFPL1	rabbit	Sigma-Aldrich	HPA014909	A117095	1:1000	

Short Name	Conjugated to	Company	Catalog no.	Lot #	Dilution
α-mouse HRP	HRP	Santa Cruz	sc-516102	F2017	1:10000
α-rabbit 800	IRDye 800CW	LI-COR	926-32213		1:5000
α-rabbit 680	IRDye 680LT	LI-COR	926-68023		1:5000
α-mouse 800	IRDye 800CW	LI-COR	926-32212		1:5000
α-mouse 680	IRDye 680LT	LI-COR	926-68050		1:5000
α-guinea pig 680	IRDye 680LT	LI-COR	926-32421		1:5000
α-guinea pig 488	Alexa Fluor 488	Invitrogen	A11073	1458631	1:1000
α-rabbit 488	Alexa Fluor Plus 488	Invitrogen	A32731	SE250296	1:1000
α-mouse 546	Alexa Fluor 546	Invitrogen	A11030	1829584	1:1000
α-mouse 647	Alexa Fluor 647	Invitrogen	A21235	1511346	1:1000
α-mouse 647	Alexa Fluor Plus 647	Invitrogen	A32728	SE250294	1:1000

Table S2. TA-proteins pulled-down with the c-Myc-TRC40$_{D74E}$ construct analysed by mass-spectrometry.

UniProt ID	Protein name	Gene symbol	p value	log2 (Fold change)
VAPB_HUMAN	Vesicle-associated membrane protein-associated protein B/C	VAPB	0.0002	1.2995493
EMD_HUMAN	Emerin	EMD	0.0007	1.2408614
VAMP7_HUMAN	Vesicle-associated membrane protein 7	VAMP7	0.0008	2.3780926
GOGB1_HUMAN	Golgin subfamily B member 1 (Giantin)	GOLGB1	0.0035	-1.7250403
LAP2B_HUMAN	Lamina-associated polypeptide 2, isoforms beta/gamma	LAP2	0.0057	0.5583429
K7ESP4_HUMAN	Dephospho-CoA kinase domain-containing protein	DCAKD	0.0220	1.1499333
UB2J1_HUMAN	Ubiquitin-conjugating enzyme E2 J1	UBE2J1	0.0241	1.3633126
STX5_HUMAN	Syntaxin-5	STX5	0.0475	1.0932206
CDKAL_HUMAN	Threonylcarbamoyladenosine tRNA methylthiotransferase	CDKAL1	0.0753	0.8713599
MAVS_HUMAN	Mitochondrial antiviral-signaling protein (MAVS)	MAVS	0.2301	0.5362815
INP4A_HUMAN	Type I inositol 3,4-bisphosphate 4-phosphatase	INPP4A	0.5117	0.363725
MCL1_HUMAN	Induced myeloid leukemia cell differentiation protein Mcl-1	MCL1	0.5297	0.7643984
E7EST9_HUMAN	Ubiquitin carboxyl-terminal hydrolase 19	USP19	0.5301	0.6081325
Q96NX8_HUMAN	Syntaxin-16D	STX16	0.5515	0.408667
LRC59_HUMAN	Leucine-rich repeat-containing protein 59	LRRC59	0.6505	0.3805235
FA98B_HUMAN	Protein FAM98B	FAM98B	0.8603	0.180839
FIS1_HUMAN	Mitochondrial fission 1 protein	FIS1	0.8610	-0.0717239
GOGA5_HUMAN	Golgin subfamily A member 5 (Golgin-84)	GOLGA5	0.9002	0.0384847

Table S3. Peptides obtained in MS and used for quantitation of statistically significant TA-proteins pulled-down with c-Myc-TRC40 constructs.

UniProt ID	Protein Name	Gene Symbol	Peptides used for Quantitation	Position	Unused Score	Total Score	Seq. Cov. [%]	PSMs > 95%
O95292	Vesicle-associated membrane protein-associated protein B/C	VAPB	SLSSSLDDTEVKK	156-68	17.72	17.74	51.8	11
			TVQSNSPISALAPTGK	201-216				
			VEQVLSLEPQHELK	4-17				
P50402	Emerin	EMD	DSAYQSITHYRPVSASR	158-174	12.68	12.72	25.2	9
			IFEYETQR	38-45				
			YNIPHGPVVGSTR	19-31				
P51809	Vesicle-associated membrane protein 7	VAMP7	AILFAVVAR	2-10	5.74	5.80	15.0	3
Q9Y385	Ubiquitin-conjugating enzyme E2 J1	UBE2J1	LSTSPDVIQGHQPR	265-278	8.43	8.45	21.1	4
P42166	Lamina-associated polypeptide 2, isoform alpha	LAP2	EATQILSVPK	526-535	77.05	77.21	65.0	55
			EPLVATNLPGR	254-264				
			ETTTGYYKDIVENICGR	316-332				
			GGTLFGGEVCK	675-685				
			QSQHDKIDASELSFPFHESILK	479-500				
			SGIQPLCPER	335-344				
			TVVSHSLTTLGLEVAK	463-478				
			VIEEEWQQVDR	501-511				
P42167	Lamina-associated polypeptide 2, isoforms beta/gamma	LAP2	GAAGRPLELSDFR	369-381	6.80	32.12	37.2	21
			GGPLQALTR	240-248				
			YVPLADVK	394-401				
K7ESP4	Dephospho-CoA kinase domain-containing protein	DCAKD	INAQLPLTDK	159-168	2.07	2.08	10.5	1
Q13190	Syntaxin-5	STX5	APVSALPLAPNHLGGGAVVLGAESHASK	214-241	26.08	26.16	45.1	17
			AVEIEELTYIIK	129-140				
			DLSNTFAK	104-111				
			DRTQEFLSACK	59-69				
			HLQTHSNTIVVSLQSK	167-182				
			NTDQGVYLGLSK	11-22				
			QIAQLQDFVR	149-158				
			YFQSVTSNR	325-333				
Q14789	Golgin subfamily B member 1	GOLGB1	AQVVDLLQQELTAAEQR	272-288	72.13	72.31	22.6	34
			GLTAQIQSFGR	2728-2738				
			SAAQPSTSPAEVQSLKK	2865-2881				

Unused Score: Sum of -log (confidence) values of all peptides per protein which is not claimed by other, non-overlapping hypotheses.
Total Score: Sum of -log (confidence) values of all peptides per protein.
PSMs >95%: number of primary sequences per protein substantiated by >95% confidence matches